Cargo Ships & Coastal Smog: A Case Study of San Pedro Bay

Philip Economides*

Texas Tech University

July 24, 2025

Abstract

Vessel queuing procedures at maritime ports may induce strategic changes in the polluting activities of transport operators. This paper documents a reduction in vessel emissions following the introduction of San Pedro Bay's new ETA-based queuing system. Using geospatial vessel position data in monitored US coastal areas, alongside records of vessel departures at foreign ports of origin, I show that the global emissions of containership voyages servicing Los Angeles and Long Beach declined, on average, by 10%. The added certainty of vessel admittance times incentivized ships to slow their voyage speeds and strategically limit local wait times. However, guaranteed queue positions also attract greater commercial activity, which led to an overall deterioration in local air quality, despite per-vessel emissions falling.

JEL Codes: D62, F18, F64, L51, Q52, Q53, R41
Keywords: local environmental policy, transport externalities, local air pollution, port logistics, vessel queues, congestion, maritime trade.

*Department of Economics, Texas Tech University. Contact: peconomi@ttu.edu

I am indebted to Woan Foong Wong, Bruce Blonigen, Anca Cristea, and Nicole Ngo for their advice and guidance. I would also like to thank Max Auffhammer, Mark Colas, Hamid Firooz, Jacob Gellman, Jamie Hansen-Lewis, Grant McDermott, Emmett Reynier, Ed Rubin, as well as seminar participants at the AERE-organized sessions of WEAI 2025, the Midwest Economic Theory and International Trade Conference, and the AERE@OSWEET online forum for their suggestions and comments. I appreciate the generous funding the Division of Graduate Studies at the University of Oregon provided through the 'Thesis and Dissertation Award', which financed my access to port call data from MarineTraffic. All remaining errors are my own.

1. Introduction

In the final months of 2021, the image of dozens of container ships idling off the coast of Southern California became a symbol of pandemic-era supply chain breakdowns. Nowhere was this congestion more visible than in the San Pedro Bay port complex, the combined operations of the Ports of Los Angeles and Long Beach. Together, this commercial hub receives 40 percent of US containerized imports. Yet behind the headline-grabbing gridlock, a subtle environmental issue developed. Vessel congestion and extended idling outside the ports came with a surge in local air pollution. The operational protocols that had governed vessel arrivals for decades had inadvertently shifted an environmental externality, normally concentrated near port terminals, onto coastal communities and ecosystems.

This paper investigates a recent logistical intervention aimed at mitigating local externalities associated with vessel congestion, the introduction of an estimated time of arrival (ETA) based vessel queuing system for container ships visiting Los Angeles and Long Beach. The new queuing system was announced and implemented within a five-day window in November 2021, offering little time for advanced behavioral adjustment by shipping firms or carriers. This abrupt rollout created conditions well-suited for a quasi-experimental research design, enabling causal inference by comparing outcomes before and after the policy among treated and control ports.

This decision replaced the longstanding "first-come, first-served" queuing protocol with a new system that allocates queue positions based on each vessel's estimated arrival time upon departure from a prior port. By removing the incentive to race toward port, and influence queue position, an ETA system may encourage vessels to slow their transit, reducing congestion and offshore anchorage accumulation. Additionally, the new system mandates that vessels remain 150 nautical miles offshore while awaiting admittance, rather than queuing in the shallow bay area. This second detail potentially increases fuel consumption due to greater vessel repositioning and a need to counter stronger open-sea currents. The policy was designed to improve navigational safety, streamline vessel flow, and curb emissions from idling ships near densely populated coastal regions. I study how this operational shift altered vessel behavior, with particular emphasis on changes to queuing dynamics, emissions intensity, and ambient air quality in adjacent communities.

The environmental costs of maritime trade have received growing attention in recent years. While global shipping accounts for approximately 3 percent of carbon emissions (IMO, 2021), it is a disproportionately large contributor to localized air pollutants such as NO_X, SO_2, and $PM_{2.5}$, particularly in coastal urban areas.

Maritime transportation of goods has also grown dramatically, further concentrating these damages. From 1965 to 2020, the cargo weight of short-distance maritime trade increased by 45 percent, while long-haul shipping more than doubled (Ganapati and Wong, 2023). Approximately 70 percent of maritime emissions are released within 400 kilometers of coastlines (Corbett et al., 2007), exacerbating health risks in nearby populations, including elevated asthma rates, cardiopulmonary disease, and premature mortality (Capaldo et al., 1999; Liu et al., 2016; Gillingham and Huang, 2021; Zhang et al., 2021). Yet empirical identification of these effects has been hindered by the diffuse spatial and temporal structure of shipping activity, as well as the presence of other emission sources near ports. By leveraging a quasi-experimental change in port queuing practices, in which concentrated environmental exposure occurs offshore and is subsequently relaxed, this paper provides a rare opportunity to causally link operational logistics to localized environmental outcomes.

The analysis proceeds in three stages. First, I construct a high-frequency panel of containership activity by matching global port call records with minute-level vessel position (AIS) data. This allows me to decompose each voyage into distinct stages: oceanic transit from the prior port of origin, queuing behavior upon entering US waters, and port admittance. Using vessel identifiers and geospatial overlays, I isolate international voyages to the West Coast and measure each ship's transit speed, queuing duration, and movement path. Second, I estimate transit emissions during voyage and queuing stages by combining vessel-specific fuel consumption functions (indexed by speed and capacity) with pollutant-specific emission factors. Third, I use a difference-in-differences strategy to quantify the causal effect of the queuing policy's implementation on vessel emissions. Importantly, the expected treatment effect is ambiguous ex ante. Vessels may reduce voyage-phase emissions due to slower transit but may also incur greater emissions offshore due to repositioning and extended queuing farther from shore.

I find that the policy encouraged a slowdown in vessel transit of 17 percent, resulting in a 10.5 percent decline in voyage-phase emissions. It also reduced the average vessel's offshore queuing duration and associated emissions by approximately 34 percent and 26 percent, respectively. However, during post-policy queuing, hourly emissions rose by 11.6 percent, suggesting that the countervailing effect of open-sea repositioning partially offset the system's environmental gains. Taking both voyage and queuing effects into account, I estimate an overall 11.2 percent decline in global emissions from containerships inbound for San Pedro Bay attributable to the new queuing system. Despite these reductions in per-vessel emissions, ambient pollution levels near the ports increased following the policy's implementation. Upon pairing

my findings with AP3, an integrated assessment model that links air pollution to monetary damages in the United States, I estimate that this policy introduced environmental costs of $155-474mn. This contrast between declining emissions intensity and rising total pollution illustrates a central policy dilemma. Gains in logistical efficiency do not always translate into reductions in cumulative environmental damage. In high-traffic freight environments, per-unit improvements can be outweighed by scale effects, particularly if reforms enhance the commercial competitiveness of treated locations. I document that the ports of Los Angeles and Long Beach experienced a relative increase in commercial throughput of approximately 20 percent compared to other major West Coast facilities. These patterns suggest that improvements in queuing efficiency enhanced the ports' competitive appeal, drawing additional vessel traffic, on-site vehicle activity, and intermodal freight movement. As a result, although the carbon intensity per unit of transported goods declined, the total volume of on-site activity likely offset those gains. This highlights the importance of disentangling improvements in operational efficiency from changes in cumulative environmental impact.

This paper contributes to several strands of literature. First, it adds to studies leveraging use of relatively modern transportation data (Heiland et al., 2019; Prochazka et al., 2019; Tumbarello et al., 2019; Brancaccio et al., 2020; Wong, 2022; Wong and Fuchs, 2022; Molina et al., 2024). The precision of automatic identification system (AIS) data allows for the analysis of emissions control areas, vessel routing, and slow steaming behavior (Klotz and Berazneva, 2022; Scott and Mayer, 2023). I apply a novel approach that infers vessel-level emissions by combining AIS data with international port call records and pollutant conversion factors. This approach enables high-resolution estimates of localized emissions to evaluate the environmental and trade consequences of queue reordering, an area still underexplored in research dovetailing topics of energy, environment, operational research.

I also contribute to topics of transport congestion, environmental externalities, and pollution regulation (Auffhammer and Kellogg, 2011; Kinney et al., 2011; Cristea et al., 2013; Ngo et al., 2015; Shapiro, 2016; Rivera, 2021). Gillingham and Huang (2021) finds that at-berth emissions in US ports contributed to reduced childbirth weights. Similarly, Hansen-Lewis and Marcus (2022) concludes that US maritime emissions control areas significantly decreased fine particulate matter, low birth weight, and infant mortality. I complement these studies by analyzing a logistical intervention that reduces emissions without imposing direct regulatory costs on shippers. I isolate the effect of the introduction of an ETA-based queuing system, controlling for strategic port switching, and highlight a sizable local emissions

reduction attributed to decreased vessel idling. While limited to narrow geographic regions, I also show that this stage of transit represents between $10 - 50\%$ of total transport time for inbound containerships along the US West Coast.

Third, I inform ongoing policy debates on maritime decarbonization. The International Maritime Organization (IMO) aims to cut global shipping emissions by 20-30 percent by 2030 and by at least 70 percent by 2040. Similarly, the U.S. Department of Transportation's National Blueprint for Transportation Decarbonization calls for cleaner fuels and operational reforms across freight modes.[1] I add to the policymaker toolkit by evaluating how low-cost adjustments in queuing procedures could reduce maritime emissions. I show that queue restructuring can meaningfully reduce emissions while boosting port throughput, a rare alignment of environmental and economic objectives. While small or uncongested ports may not experience similar gains, large gateways with substantial queuing delays could benefit from analogous procedural reforms. Ludwig (2025) warns that maritime carbon taxes may depress port competitiveness. My findings highlight an alternative pathway to emissions reductions with positive or neutral effects on throughput.

The remainder of the paper proceeds as follows. Section 2 outlines the institutional background of the queuing policy. Section 3 describes the data sources and emissions estimation methodology. Section 4 presents the empirical strategy and main results on transit behavior, emissions, local air quality, and port activity. Section 5 estimates the monetary consequences of emission level adjustments in the San Pedro Bay area. Section 6 concludes.

2. Background

The sharp rebound in U.S. consumer demand during the COVID-19 recovery led to an unprecedented surge in maritime imports. Between October 2020 and November 2021, inbound container traffic to the United States rose by over 15 percent year-on-year, more than four times the average annual growth rate over the prior decade.[2] The San Pedro Bay port complex, comprising the Ports of Los Angeles and Long Beach, bore the brunt of this volume increase. As a result, the number of containerships anchored offshore ballooned, leading to historically high congestion and environmental strain.

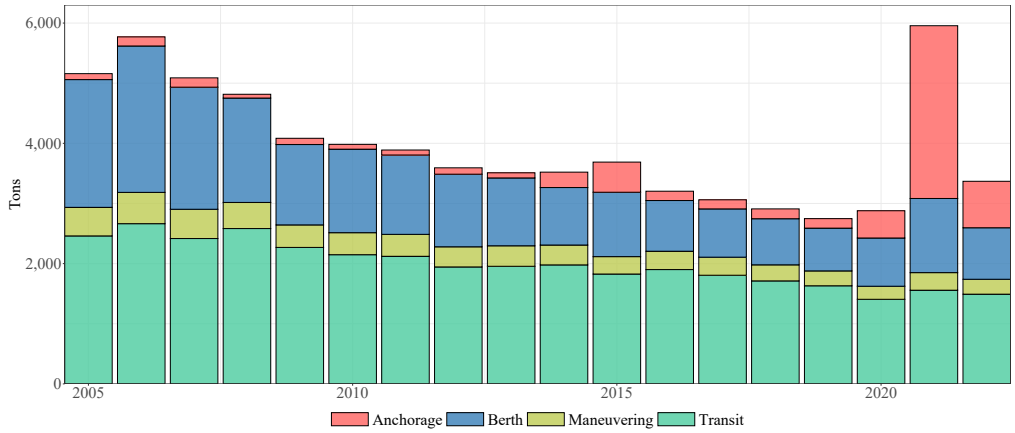
This bottleneck had a marked impact on regional air quality. According to

[1] Available at https://www.transportation.gov/priorities/climate-and-sustainability/us-national-blueprint-transportation-decarbonization. Accessed May 30, 2024.

[2] Author calculations using US Customs and Port Authority data.

the Los Angeles Port Authority's Inventory of Air Emissions (2021), total emissions of NO_X rose by over 69 percent between 2020 and 2021, with emissions from ocean-going vessels increasing by 143 percent. The anchorage and queuing phases – normally a minor component of total emissions – became dominant contributors (Figure 1), with containerships accounting for the majority of this growth (Figure 2).

Figure 1: NOx Emissions (tons), by mode



Source: Los Angeles Port Authority's Inventory of Air Emissions (2021, 2022).

The environmental risks of this congestion were not hypothetical. In October 2021, just weeks before a policy overhaul, a crude oil pipeline off the coast of Orange County was ruptured by the anchor drag of a waiting containership. Cleanup and damages came at an estimated $160 million price tag.[3]

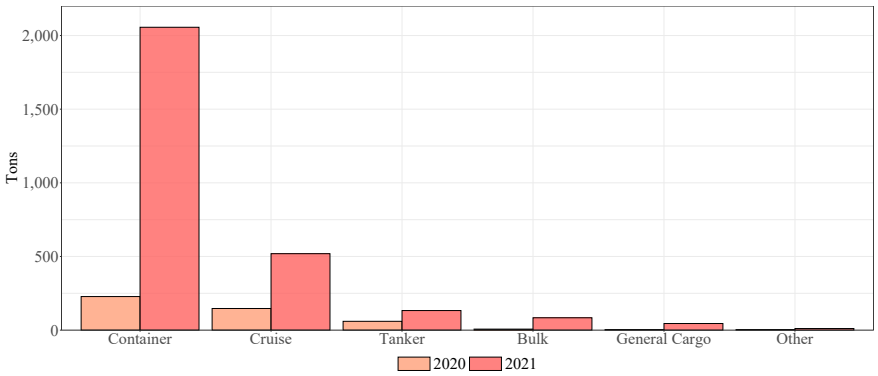
In response to these operational and environmental pressures, the ports of Los Angeles and Long Beach introduced a major procedural reform on November 11, 2021. Under the new system, berth access would be assigned based on each vessel's estimated time of arrival (ETA), rather than physical arrival order. This adjustment, coordinated through Pacific Maritime Management Services, marked a departure from the traditional first-come, first-served protocol. Additionally, vessels were instructed to remain outside a newly established "Safety and Air Quality Area," defined as a radius 150 nautical miles from the port area and 50 nautical miles from Southern Californian coastlines, while awaiting berth assignment.

ETA-based queuing and open-sea idling jointly define the policy effect studied in this paper. Their net environmental effect is ambiguous a priori. On one hand, guaranteed berth access could reduce strategic early arrivals and incentivize slower travel speeds, thus lowering emissions during the voyage phase. On the other, greater

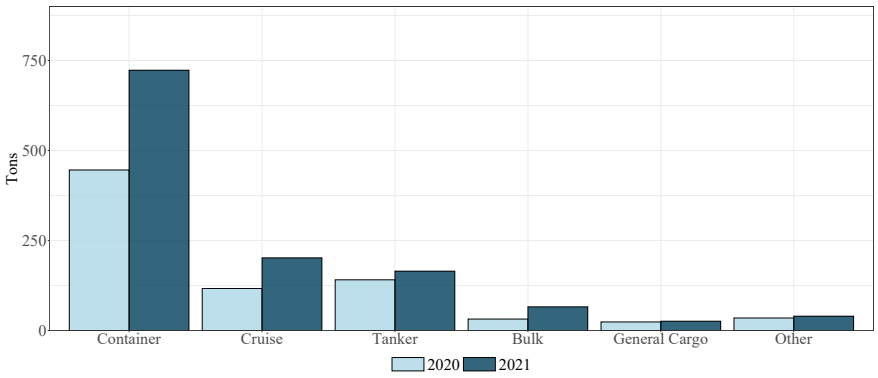
[3]See NTSB Report MIR-24-01, "Anchor Strike of Underwater Pipeline and Eventual Crude Oil Release," Project DCA22FM001.

Figure 2: NoX Emissions by Vessel Type and Mode

(a) Anchorage



(b) Berth (At Dock)



Source: Los Angeles Port Authority's Inventory of Air Emissions (2021).

queuing distances and exposure to oceanic currents could increase idling emissions during the anchorage phase. The ultimate impact hinges on the relative magnitude of these opposing forces. If vessels hardly changed their speeds and fuel consumption while remaining adrift off the continental shelf is particularly taxing on emission levels, this policy could be considered a form of environmental NIMBY-ism, similarly to cases featured in Morehouse and Rubin (2021) and Zou (2021).[4] In this case, ports would be reaping the commercial benefits of their property rights while exporting the cost of any resulting air pollution. Alternatively, suppose speed reductions are considerable or vessels spend less time idling due to improved certainty on port admittance. In that case, the greater fuel expended during the queuing process may be negligible in comparison. Under such circumstances, this logistical practice may

[4] "Not In My BackYard", a term coined by Mitchell and Carson (1986). Often associated with cases in which a property owner wants a beneficial economic activity to occur on her property while expelling the negative externalities of production elsewhere.

offer oversight bodies, such as the IMO or DOT, an additional policy tool through which to meet the long-term goals of a decarbonized maritime transport sector.

Evaluating the consequences of this queuing reform requires detailed data on vessel movements, emissions behavior, and local air quality patterns. To this end, I assemble a novel dataset that links automatic identification system (AIS) records of ship activity with port call schedules, emission factor models, and monitor-level pollution readings. The next section describes the construction of this dataset, outlining how I infer vessel-level emissions from movement logs and how I map these to environmental exposure in affected regions.

3. Data & Inference

This section describes the construction of a dataset that links vessel movement, geographic boundaries, and local air quality to assess the emissions impact of the San Pedro Bay queuing reform. I combine publicly available records and proprietary data to construct a panel of individual vessel transits and associated emissions between November 2019 and November 2022. Full details on matching procedures, data cleaning, and emissions derivation are provided in the Data Appendix.

3.1. Vessel Movement Data

Port call data were obtained from MarineTraffic (MT), which provide port entry and exit records for individual vessels. I focus on port visits across major U.S. West Coast ports – Los Angeles, Long Beach, Oakland, Seattle, and Tacoma – over the period November 2019 to November 2022. Each record includes timestamps and geolocations for port arrivals and departures, as well as unique vessel identifiers via International Maritime Organization (IMO) codes.

To differentiate between active transit and queuing periods near the US coast, I integrate MT records with high-frequency location signals from the US Coast Guard's AIS (Automatic Identification System), accessed via MarineCadastre (MC). This AIS data provides minute-level records of individual vessel speed, location, and status within US waters.

Time-invariant ship characteristics were sourced from VesselTracking (VT), including gross tonnage and container capacity (TEU). These attributes are used to infer fuel consumption by vessel type and voyage profile. Vessels are matched across both sources using IMO codes and voyage timelines. A summary of the matching logic and queuing definitions is presented in section I of the Data Appendix.

The cleaned dataset includes 10,035 port visits serviced by 1,061 distinct containerships, some of which are short transits between US ports. Removing these vessels and shifting attention to international journeys exclusively brings the sample to 5,785 visits, serviced by 990 distinct containerships. Table 1 summarizes vessel and voyage characteristics by port and time period.

Table 1: Summary Statistics of Vessel Voyages

Port	Period	Visits	Vessel Age	Max TEU	Dwell Time	Voyage Time	Voyage Speed
Long Beach	pre-	1445	10.55	7955.11	99.60	263.27	19.15
Long Beach	post-	647	11.29	7843.69	107.14	360.22	15.84
Los Angeles	pre-	1778	10.59	7581.44	118.53	276.32	19.49
Los Angeles	post-	746	10.83	7419.38	135.44	402.57	15.48
Oakland	pre-	179	12.61	5019.64	48.72	253.46	18.55
Oakland	post-	181	14.07	3411.29	72.67	324.90	15.75
Seattle	pre-	162	12.50	6118.45	68.32	288.18	17.04
Seattle	post-	203	13.19	5869.30	63.61	351.39	15.01
Tacoma	pre-	355	11.70	7354.04	75.75	322.64	16.23
Tacoma	post-	119	12.07	8223.23	127.71	472.65	12.77

Columns 4–8 report averages across vessels engaged in international transit towards the US west coast for a given major port and sample time window. "Pre-" is defined as prior to November 11th 2021, when the new San Pedro Bay queuing system was announced for LA and Long Beach. 'Vessel Age' is reported in years. 'Max TEU' reports the container capacity of vessels, 'Dwell Time' reports the average hours vessels spend handling goods at port. 'Voyage Time' details hours between a departure time and the point at which a vessel reappears in US waters. 'Voyage Speed' is reported in nautical miles per hour.

To address potential selection into or out of treatment, I construct an additional subsample of vessels that consistently visited the same ports before and after the policy. I exclude vessels that exited West Coast service post-policy, entered the sample only after the policy, or switched destination ports ("switchers"). This balanced panel comprises 2,418 port visits by 301 vessels.

3.2. Geographic and Trade Data

Port boundaries are defined using Port Statistical Area shapefiles from the U.S. Army Corps of Engineers (USACE). These geographic polygons are used to delineate port regions and to calculate vessel queuing durations based on AIS signals.

To measure port-level trade activity, I compile a novel monthly panel of bilateral container flows from individual port authorities through direct requests and FOIA submissions. These data capture loaded and empty container inflows and outflows, covering over 80% of national container throughput (Economides, 2024). Additional trade value and volume measures are obtained from USA Trade Online and restricted to containerized flows at the five focal ports.

3.3. Air Quality Data

Daily air quality readings are sourced from the EPA's Air Quality Index (AQI) database. Monitors report concentrations of PM2.5, PM10, CO, SO_2, and NO_2, and are distributed across both coastal and inland sites in California and other West Coast states. Monitor placement is determined by state authorities in accordance with federal siting and quality standards.

To identify localized impacts, I assign monitors to treatment and control zones based on their proximity to port centroids. Zone I includes monitors within 25 miles of a port, while Zone II includes those 25–50 miles away. These distance bands follow the precedent established by Gillingham and Huang (2021), who identify significant effects of port emissions on ambient air quality and health outcomes within these radii. I implement this classification using a 'ring method' approach, detailed in Section 4.1.[5]

3.4. Fuel Consumption and Emissions Inference

Vessel emissions are inferred by estimating fuel consumption as a function of ship size (TEU capacity) and average travel speed. I interpolate fuel use values from TEU-specific curves presented in Rodrigue (2020), and fit a polynomial function using OLS. Due to known measurement issues at low speeds, I apply a correction factor for sub-cruise transits, following prior studies. See Appendix A3 for a full derivation.

I use fuel consumption use estimates, combined with conversion factors from Czermański et al. (2021), to generate emission levels (CO_2, SO_x, NOx, PM2.5) for individual vessel-vovyages, both at during the voyage and queuing stages of transit. I assume full compliance with IMO 2020 sulfur standards, which defers attention exclusively to the use of MDO 0.5% fuel, featured in Table 2.

To evaluate the environmental implications of this policy, I construct a high-frequency dataset that links vessel movements, port operations, and emissions across key stages of maritime transit. This allows for a detailed comparison of behavior and environmental outcomes before and after the queuing reform.

[5] As a robustness check, I incorporate wind direction data from nearby NOAA stations to examine whether pollution effects are more pronounced on days when wind is directed from anchorage zones toward populated inland areas. See Appendix A4 for details.

Table 2: Emissivity Indices for Selected Marine Fuels

Fuel	[kg/t of Fuel] CO_2	SO_X	NO_X	$PM_{2.5}$
MDO 0.5%	3206.00	10.50	50.50	2.30
HFO 1.5%	3114.00	31.50	51.00	3.40
HFO 2.0%	3114.00	42.00	51.00	3.40
HFO 3.5%	3114.00	71.50	51.00	3.40
LSHFO 0.5%	3151.00	10.50	51.00	2.30
LSMGO 0.1%	3151.00	2.10	50.50	2.30
LNG	2750.00	¡0.02	8.40	0.02
Methanol	1375.00	0.00	26.10	0.02
HFO + SCRUBBER + SCR	3176.00	0.84	7.65	0.51

Source: Czermański et al. (2021), based on the assumptions of the Med Atlantic Ecobonus (MAE) Project, MAE External Cost Calculator Tool.

4. Empirical Strategy & Results

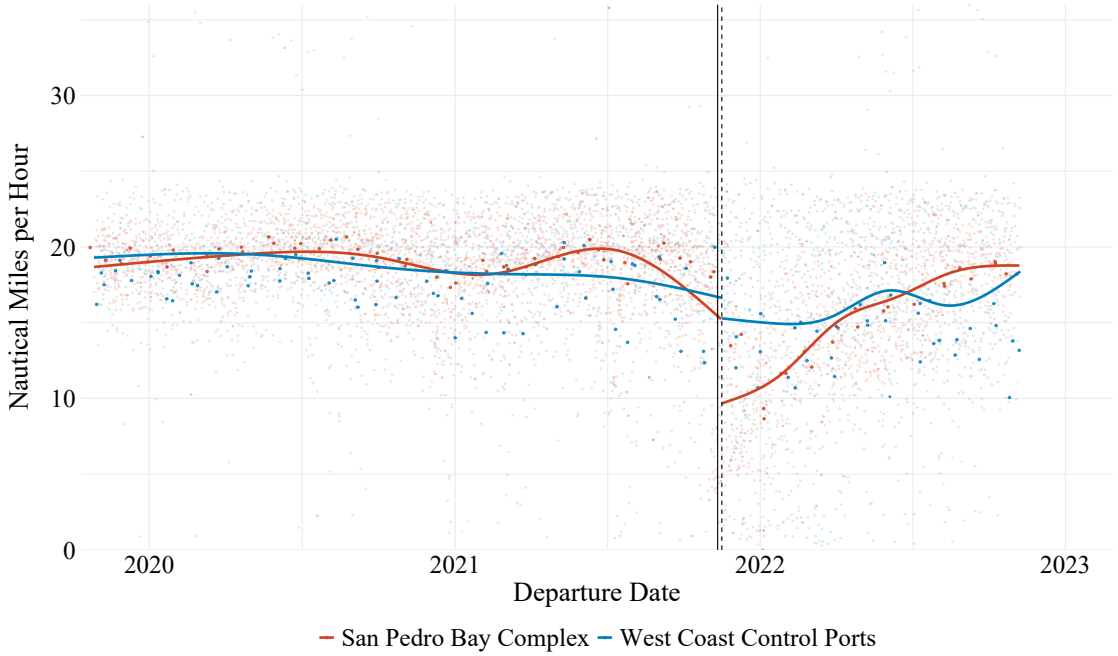
Having constructed a granular dataset that traces vessel movements across distinct transit phases, I now estimate the causal impact of the San Pedro Bay queuing reform on emissions intensity and environmental exposure. Upon establishing an identification strategy, the empirical analysis proceeds in three stages. First, I estimate how the reform altered vessel behavior and emissions intensity during voyage and queuing phases. Second, I aggregate these phase-specific effects to quantify changes in global emissions per vessel arrival and show that, despite the narrow geographic scope of queuing, it accounts for a substantial share of total transit time and emissions. Finally, I examine localized air quality outcomes and port throughput to assess whether operational gains translated into broader environmental and economic impacts. This structure allows me to distinguish direct improvements in vessel efficiency from systemic shifts in port activity, illustrating how logistical reforms can shape both emissions intensity and cumulative pollution burdens.

4.1. Identification Strategy

To estimate the causal effect of the San Pedro Bay queuing reform on vessel behavior and emissions, I employ a difference-in-differences (DiD) design. The treatment group consists of container ships serving the ports of Los Angeles and Long Beach, where the reform was jointly announced and implemented between November 11th and 16th, 2021. I compare outcomes at these ports to a set of untreated West Coast ports, Oakland, Seattle, and Tacoma. These maritime hubs were not subject to analogous queuing policies. These ports serve as counterfactuals due to their geographic proximity, similar trade exposure, and concurrent experience of pandemic-era macroeconomic shocks.

The DiD framework is well-suited to this setting for three reasons. First, the timing of the reform offers a quasi-experimental setup. The new queue system was announced and implemented within a five-day window, minimizing the scope for anticipatory behavioral responses. Second, treated and control voyages exhibit parallel trends in key pre-treatment outcomes, such as voyage speed, supporting the assumption that their emission trajectories would have evolved similarly in the absence of the reform (Figure 3).[6] COVID-related disruptions to vessel movements and port congestion occurred near-simultaneously across West Coast ports, as documented in contemporaneous shipping bulletins and maritime traffic reports. I exclude Gulf and East Coast ports, which faced lagged or regionally distinct recovery dynamics.

Figure 3: Parallel Trends in Voyage Speeds



Note: Containership voyage speeds destined for San Pedtro Bay (red) and control the ports of Seattle, Tacoma, and Oakland (blue). Vertical solid line marks first earliest announcement of the new queuing system (November 11, 2021). Vertical dashed line marks the start of the system's implementation (November 16, 2021). Solid lines show separately estimated restricted cubic spline functions for the periods before and after the queueing system implementation, and within San Pedro Bay and control port areas. The panel y axis has been truncated at 36 to aid visual inspection, though the spline functions are estimated on the full sample of observations.

Third, I mitigate concerns about endogenous port choice or selective entry by constructing a balanced panel of vessels that consistently served the same ports before and after the policy. This approach excludes route "switchers" and new entrants whose selection into specific port networks may be correlated with treatment timing. For example, in response to the reform, a vessel might initially set course for Oak-

[6]See Appendix Section B1 for further evidence of the parallel trends assumption being satisfied.

land to manipulate its position in the virtual queue before ultimately rerouting to Los Angeles. If such strategic routing were widespread among new or switching vessels, it would bias the estimated treatment effect downward, understating the true extent of post-policy slow steaming and overstating the resulting efficiency gains. By excluding potential switchers, entrants, and exiters, I ensure that the estimated treatment effects reflect behavioral adjustments among a stable set of vessels.

While pre-treatment vessel characteristics differ modestly across ports (Table 1), the DiD design does not require equivalence in levels. I instead require stability of those inherent differences over time. Including vessel–route fixed effects (ϕ^S_{io}) absorbs persistent variation in vessel size, age, and route-specific behavior, while time fixed effects (ϕ^S_t) absorb time-varying shocks common to all ports, such as fuel prices, holiday effects, or macroeconomic disruptions. To further address concerns about differential pandemic recovery trajectories, the inclusion of ϕ^S_t ensures that any regionally common or global COVID shocks are accounted for.[7] This structure supports identification via within-day comparisons between treated and control vessels operating under otherwise similar conditions.

I measure emissions intensity by stage of transit. Vessels in US waters are assigned status codes indicating whether they are underway (U), maneuvering (M), at anchor (A), or at berth (B). I define local emissions efficiency as emissions per hour of activity across these stages. Using local emissions efficiency – represented by emissions per hour $\left(\frac{e^L_{ipt}}{h^L_{ipt}}\right)$ – summed across these four local transit stages,

$$\frac{e^{\mathrm{L}}_{ipt}}{h^{\mathrm{L}}_{ipt}} = \frac{e^{\mathrm{U}}_{ipt} + e^{\mathrm{M}}_{ipt} + e^{\mathrm{A}}_{ipt} + e^{\mathrm{B}}_{ipt}}{h^{\mathrm{U}}_{ipt} + h^{\mathrm{M}}_{ipt} + h^{\mathrm{A}}_{ipt} + h^{\mathrm{B}}_{ipt}}, \tag{1}$$

I aggregate the underway, maneuvering, and anchoring stages into a "queuing" stage (Q) and analyze it separately from berthing. To measure global emissions, I take these measures jointly with voyage (V) emissions of each ship from their respective ports of departure, e^V_{ipt}. Global emissions efficiency is then defined as

$$\frac{e^{\mathrm{G}}_{ipt}}{h^{\mathrm{G}}_{ipt}} = \frac{e^{\mathrm{V}}_{ipt} + e^{\mathrm{Q}}_{ipt}}{h^{\mathrm{V}}_{ipt} + h^{\mathrm{Q}}_{ipt}} \tag{2}$$

To exploit the quasi-experimental nature of this policy change – announced and

[7] Examples include labor availability, fuel constraints, and seasonal congestion.

introduced within a 5-day window – I use the following DiD specification:

$$Y_{iodt}^{S} = \delta_1^S T_d + \delta_2^S D_t + \delta_3^S \left(T_d \times D_t\right) + \phi_{io}^S + \phi_t^S + \mu_{irpt}, \tag{3}$$

where i identifies the individual vessel, io indicates the vessel–voyage route serviced repeatedly over time, d represents the destination port, and t is the calendar date upon departure from port o. T_d and D_t are treatment and post-period indicators, respectively. The fuel efficiency outcome variable, Y_{iodt}^S, is emissions-per-hour on a given transit stage, $S \in \{\mathrm{V}, \mathrm{Q}, \mathrm{G}\}$ and can be decoupled for any particular stage of service. The inclusion of vessel-route fixed effects (ϕ_{io}^S) accounts for persistent differences across port pairings, while year-month fixed effects (ϕ_t^S) absorb time-varying shocks common to all ports, such as fuel price changes, seasonality in shipment volumes, or key macroeconomic events.

The coefficient of interest is δ_3^G. A negative and significant $\hat{\delta}_3^G$ would imply that the reform improved global emissions efficiency – suggesting that guaranteed queuing positions encouraged slower steaming and reduced emissions during transit. Conversely, a non-negative $\hat{\delta}_3^G$ would indicate that the emissions savings from slower steaming were offset or reversed by increased emissions during offshore idling. Referring to Eq. (2), a decline in e_{ipt}^V/h_{ipt}^V would be consistent with voyage slowdowns, while a rise in e_{ipt}^Q/h_{ipt}^Q would reflect emissions from extended idling or repositioning farther from shore. This ambiguity underscores the importance of decomposing global effects into their component stages, as well as considering broader air quality outcomes in the empirical analysis that follows.

4.2. Voyage Emission Effects

Changes in vessel voyage speed constitute a key channel through which the queuing reform may affect maritime emissions. Table 3 presents difference-in-differences estimates of the policy's effect on international voyage speeds (measured in nautical miles per hour). Each specification includes vessel–voyage and year–month fixed effects, with standard errors clustered by vessel–voyage route. Column (1) reports average treatment effects for all qualifying port arrivals. Column (2) restricts attention to voyages that do not engage in transshipment activity, defined as subsequent short-haul trips in US waters, following an international arrival. Column (3), the preferred specification, further excludes vessels that change their port-pair routing after policy implementation. This mitigates the influence of route-switching or strategic entry/exit, which may otherwise bias the estimated effects (Klotz and Berazneva, 2022). The results indicate that the policy reduced average voyage speeds

by approximately 15.9 percent in the preferred specification.[8] This substantial decline in travel velocity suggests that vessels altered operating behavior, potentially through speed reduction strategies, to comply with the new queue system.

Table 3: Difference-in-Difference Estimates – Voyage Speed

	Nautical Miles Per Hour		
	(1)	(2)	(3)
Post–Policy	0.2489***	0.2215***	0.2509***
	(0.0606)	(0.0783)	(0.0926)
Treatment	0.0453**	0.0423*	0.0788
	(0.0228)	(0.0237)	(0.1147)
DiD	-0.2091***	-0.1620***	-0.1730***
	(0.0288)	(0.0330)	(0.0398)
Vessel–Voyage FE	✓	✓	✓
Year–Month FE	✓	✓	✓
Observations	7,192	5,785	2,418
Average Speed, Pre-Policy	18.98	19.14	19.65
R^2	0.85	0.71	0.62

Note: ***: 0.01, **: 0.05, *: 0.1. Standard-errors are robust to clustering within vessel–voyage lanes of transport service. Each observation is a distinct voyage arriving on the US west coast between Nov 2019 and Nov 2022. Column 1 reports the broad diff-in-diff treatment effect on vessels. Column 2 excludes transshipping activity – short subsequent journeys between US ports after their initial arrival from a foreign port of origin. Column 3 only includes Column 2 vessel voyages that maintained the same international trade routes pre- and post- policy. Each regression uses a logged dependent variable. To limit extreme outlier distortions, I exclude any voyages with travel speeds less than the 25th percentile minus three times the interquartile range (75th percentile - 25th percentile) or higher than the 75th percentile plus three times the interquartile range (Davies and Jeppesen, 2015). "Average Speed, Pre-Policy" refers average vessel voyage travel speed destined for treated US ports before 11/11/2021.

Table 4 reports the policy's impact on total and normalized CO_2 emissions. Focusing on international voyages with no transhipping, Column (2) reports a 9.2 percent reduction in voyage emissions. Column (3), which mirrors the restrictions in Table 3, provides evidence of a similar decline. In Columns (4) and (5), I shift focus to intensity-adjusted outcomes, emissions per hour and per knot traveled, respectively. These measures help assess whether emission reductions stemmed solely from longer voyage durations or also from improved fuel efficiency. Both measures show statistically significant declines of 23.4 and 8.9 percent, respectively. These findings imply that operational adjustments extended efficiency gains with respect to fuel consumption, driven by an overall slowdown in voyage speeds. Although the results are framed in terms of CO_2, the linear relationship between fuel use and other pollutant types implies similar log-differenced reductions across NO_x, SO_x, and PM emissions (Czermański et al., 2021).

I next employ an event study specification to assess the dynamic effects of the queuing reform on voyage emissions, focusing exclusively on international voyages

[8]The coefficient on the DiD term corresponds to a semi-elasticity. For a log-level regression, percentage effects are computed as $e^{\beta} - 1$.

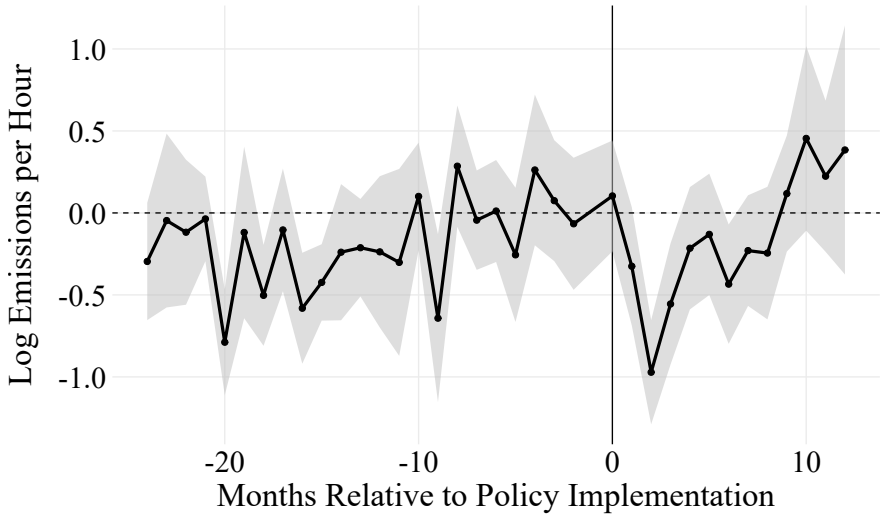
Table 4: Difference-in-Difference Estimates – Voyage Emissions

	CO_2 Emissions			Em. per Hour	Em. per Knot
	(1)	(2)	(3)	(4)	(5)
Post–Policy	0.0794	-0.0532	-0.0837	0.1356	-0.1152
	(0.0573)	(0.0780)	(0.1004)	(0.1475)	(0.0890)
Treatment	0.1043**	0.0822**	0.0784	0.1265	0.0477
	(0.0412)	(0.0364)	(0.0998)	(0.2107)	(0.0970)
DiD	-0.2073***	-0.0964**	-0.0993*	-0.2663***	-0.0932**
	(0.0305)	(0.0435)	(0.0542)	(0.0795)	(0.0468)
Vessel–Voyage FE	Yes	Yes	Yes	Yes	Yes
Year–Month FE	Yes	Yes	Yes	Yes	Yes
Observations	7,192	5,785	2,418	2,418	2,418
R^2	0.97	0.95	0.91	0.75	0.83

Note: ***: 0.01, **: 0.05, *: 0.1. Standard-errors are robust to clustering within vessel–voyage lanes of transport service. Each observation is a distinct voyage arriving on the US west coast between Nov 2019 and Nov 2022. Column 1 reports the broad diff-in-diff treatment effect on vessels. Column 2 excludes transshipping activity – short subsequent journeys between US ports after their initial arrival from a foreign port of origin. Column 3 only includes Column 2 vessel voyages that maintained the same international trade routes pre- and post- policy. Columns 4 and 5 shift focus to per hour and per nautical mile measures of emissivity, respectively. Each regression uses a logged dependent variable. To limit extreme outlier distortions, I exclude any voyages with travel speeds less than the 25th percentile minus three times the interquartile range (75th percentile - 25th percentile) or higher than the 75th percentile plus three times the interquartile range (Davies and Jeppesen, 2015).

that maintained consistent service patterns before and after the policy change. Figure 4 plots the estimated treatment effects relative to October 2021. In the immediate aftermath of the policy's implementation, vessels exhibit a temporary deceleration in transit speed, with reductions in emissions per hour that persist through mid-2022. These effects begin to attenuate after July 2022 and fully dissipate by September 2023, suggesting mean reversion in vessel behavior.

Figure 4: Event Study (TWFE) - Emissions per hour



The temporal profile of these estimates indicates that the policy's impact on long-haul voyage emissions is short-lived. While vessels initially adjust their operations in response to the ETA-based queuing system, these changes are not sustained over

time. This transient pattern implies limited potential for enduring decarbonization gains on the voyage stage of international transit. The next section shifts attention to the queuing leg of the voyage and documents a robust and persistent reduction in local emissions. When considered jointly, these findings suggest that the queuing system meaningfully reduces vessels' contribution to local air pollution, even while long-distance shipping emissions return to pre-policy norms.

4.3. Queuing Emission Effects

To isolate the emissions effect of the queuing leg of each voyage, I calculate total CO_2 emissions for each vessel while in US waters. This stage encompasses maneuvering near the continental shelf, idling offshore, and anchoring when permitted. Figure 5 illustrates the distribution of hourly emissions by treatment status before and after the policy.

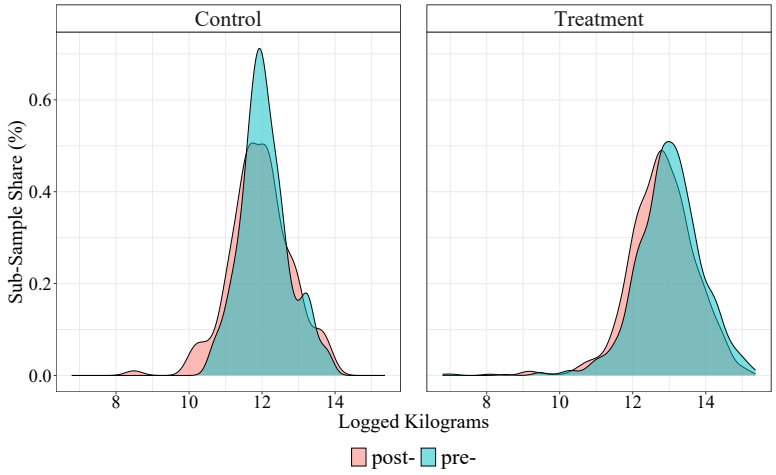
Following the introduction of the queuing system, emissions among treated vessels decline markedly, whereas no such trend is observed among control ports (Figure 5a). The increased variance among control observations is partly attributable to lower sample sizes during the post-period (Figure 5b).

I formalize these comparisons in a difference-in-differences framework (Table 5), restricting attention to vessels on stable international routes and with observable queuing data. Column 1 reveals a statistically significant 26.1% reduction in emissions during the queuing stage. This aligns with the hypothesis that increased certainty about berth availability prior to arrival reduces unnecessary offshore loitering. Columns 2 and 3 indicate that treated vessels spent less time queuing and moved at faster average speeds, suggesting a more streamlined approach to port entry. Emissions per nautical mile also fell (Column 4), consistent with more efficient engine use. Although vessels in the treatment group appear to have traveled greater distances while waiting (Column 5), the associated increase in hourly emissions (Column 6) is not statistically significant. This suggests that any increased offshore repositioning was modest and did not substantially erode the emissions gains from reduced queuing durations.

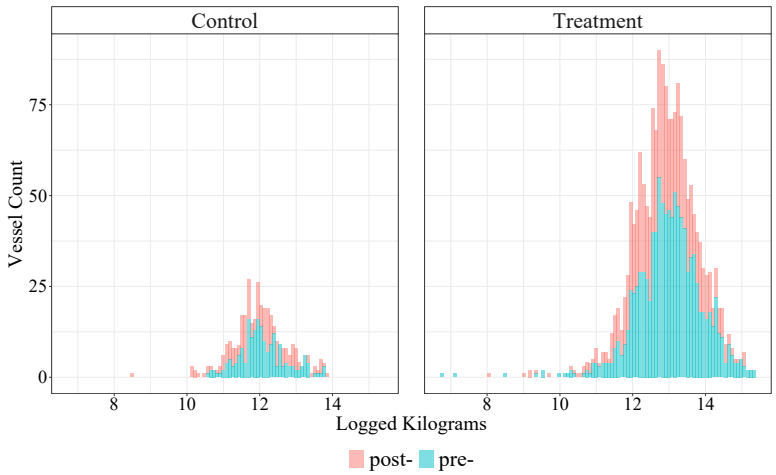
These findings underscore the local emissions benefits of the ETA-based queuing system. By reducing idle time and improving port-entry efficiency, the policy significantly cut emissions generated within US coastal waters. I next quantify how localized gains translate relative to the full course of international voyages.

Figure 5: CO_2 emissions by hour across queued vessels

(a) Distribution of Emissions by Subsample



(b) Number of Vessel-Voyages by Subsample



4.4. Global Emission Effects

To capture the full emissions impact of the queuing reform, I aggregate each vessel's voyage and queuing stages into a unified global transit measure. This approach allows for a more comprehensive assessment of environmental outcomes, extending beyond the limits of US territorial waters. As illustrated in Figure 6, queuing previously accounted for a non-trivial share of emissions, distance, and transit time for vessels calling at West Coast ports.

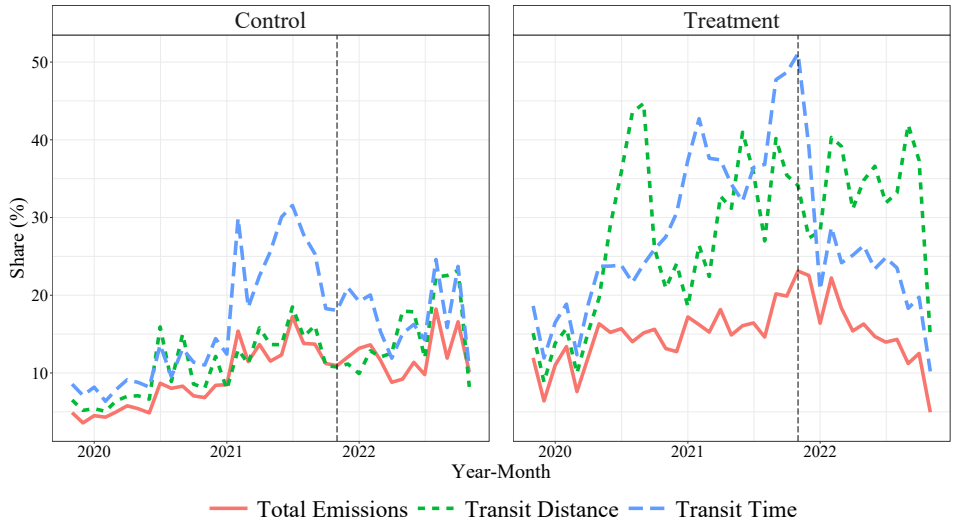
Prior to the policy's implementation, shipping congestion intensified markedly.

Table 5: Difference-in-Difference Estimates – Queuing Emissions

	CO_2 Emissions (1)	Duration (2)	Speed (3)	Em. per Knot (4)	Distance (5)	Em. per Hour (6)
Post–Period	-0.3073	-0.3294	0.2374*	0.1182	-0.4255*	0.0221
	(0.2343)	(0.2623)	(0.1416)	(0.1742)	(0.2421)	(0.1071)
Treatment	1.287***	1.586***	-0.6597***	-0.5567**	1.843***	-0.2993**
	(0.1974)	(0.2875)	(0.2068)	(0.2496)	(0.3852)	(0.1210)
DiD	-0.3046***	-0.4047***	0.2852***	-0.4341***	0.1295	0.1000
	(0.0832)	(0.1214)	(0.0781)	(0.0889)	(0.1027)	(0.0671)
Vessel–Voyage FE	✓	✓	✓	✓	✓	✓
Year–Month FE	✓	✓	✓	✓	✓	✓
Observations	2,177	2,177	2,177	2,177	2,177	2,177
R^2	0.59	0.55	0.55	0.50	0.44	0.66

Note: ***: 0.01, **: 0.05, *: 0.1. Standard-errors are robust to clustering within vessel–voyage lanes of transport service. Each observation is a distinct queuing experience of a vessel arriving on the US west coast between Nov 2019 and Nov 2022. I filter only for vessel voyages that maintained the same international trade routes pre- and post-policy and drop any observations that lack matching vessel movement data. To limit extreme outlier distortions, I exclude any voyages with emissions less than the 25th percentile minus three times the interquartile range (75th percentile - 25th percentile) or higher than the 75th percentile plus three times the interquartile range (Davies and Jeppesen, 2015).

Figure 6: Queuing Share of Global Containership Transit for US West Coast



Both treatment and control ports experienced a near tripling in queuing durations relative to total transit time. However, this trend reversed sharply only at ports adopting the ETA-based queuing system. By assigning queue positions upon departure from the prior port of call, the system curtailed offshore loitering and halted the rise in queuing's share of total travel distance. In contrast, ports outside the reform, such as Oakland, Tacoma, and Seattle, exhibited continued growth in queuing intensity through 2022.

To quantify the broader environmental implications, I estimate a difference-in-differences model combining emissions from both voyage and queuing stages (Table 6). Column 1 indicates a 10% decline in global CO_2 emissions among treated routes. Emissions per hour (Column 2) remain statistically unchanged, suggesting that the

intensity of fuel use did not fall per unit of time. However, emissions per nautical mile fell by 13% (Column 3), implying efficiency gains via reduced idling and more purposeful transit patterns.

Table 6: Difference-in-Difference Estimates – Global Emissions

	CO_2 Emissions (1)	Em. per Hour (2)	Em. per Knot (3)
Post–Period	-0.2021**	0.2380**	-0.0946
	(0.0923)	(0.1124)	(0.0932)
Treatment	0.1687*	-0.1307	-0.1836*
	(0.0897)	(0.1945)	(0.1109)
DiD	-0.1052**	-0.0298	-0.1394***
	(0.0459)	(0.0712)	(0.0491)
Vessel–Voyage FE	✓	✓	✓
Year–Month FE	✓	✓	✓
Observations	2,175	2,175	2,175
R^2	0.90	0.78	0.72

Note: ***: 0.01, **: 0.05, *: 0.1. Standard-errors are robust to clustering within vessel–voyage lanes of transport service. Each observation is a distinct global transit experience of a vessel arriving on the US west coast between Nov 2019 and Nov 2022. I filter only for vessel voyages that maintained the same international trade routes pre- and post- policy and drop any observations that lack matching vessel movement data. To limit extreme outlier distortions, I exclude any voyages with emissions less than the 25th percentile minus three times the interquartile range (75th percentile - 25th percentile) or higher than the 75th percentile plus three times the interquartile range (Davies and Jeppesen, 2015).

Although vessels slowed temporarily across the voyage leg of transit, these gains were undermined by increased repositioning activity while waiting offshore. This is consistent with the previously documented rise in queuing-stage emissions per hour. This dynamic reflects a reallocation of time. Rather than loitering aimlessly near port, vessels adjusted speeds en-route and arrived more precisely in line with assigned berthing slots. Given the added admittance certainty provided, the policy induced a shift in time allocation from uncoordinated congestion to time-optimized voyage planning.

I identify a significant reduction in vessels' carbon emissions, primarily driven by strategic behaviour in the queuing leg of vessel voyages. However, contrasting this outcome against evidence from local air quality monitors across West Coast ports highlights a prominent countervailing effect.

4.5. Local Air Quality

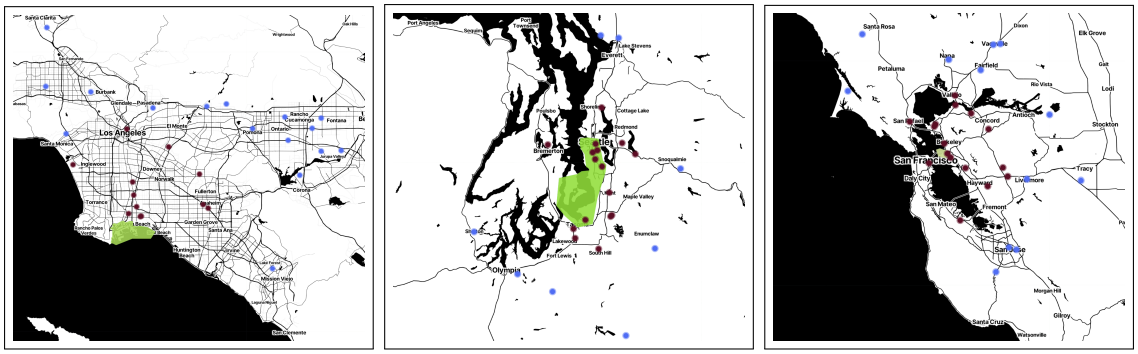
While the queuing policy yielded measurable reductions in global emissions, its impact on local air quality near ports remains less clear. This section investigates whether reduced vessel emissions in the vicinity of port areas translated into improved ambient air quality around the Los Angeles–Long Beach (San Pedro Bay) complex.

To isolate local effects, I adopt a spatial difference-in-differences approach, which compares outcomes for sites near the treatment area with those in an adjacent outer zone (Linden and Rockoff, 2008; Boarnet et al., 2017; McDermott et al., 2019; Gupta et al., 2020). Specifically, I use a "ring-method", to compare the inner radius of a region relative to a control group that represents a geospatial outer ring. Following a similar port emissions analysis by Gillingham and Huang (2021), I set the inner zone (Zone I) as a set of air quality monitors within 25 miles of the San Pedro Bay port complex centroid. The outer zone (Zone II) includes monitors located between 25 and 50 miles from the same point.

This concentric-ring approach captures near-port pollution outcomes relative to a geographically proximate, yet non-adjacent, baseline. However, if some pollutants disperse beyond the inner zone, blurring treatment boundaries, the outer ring may act as an imperfect control. To address this concern, I supplement the analysis with a second comparison. In this setting, I shift attention to monitors located within 25 miles of other major West Coast ports, which were far more likely to be unaffected by the queuing policy. The drawback of this comparison lies in its inability to account for region-specific shocks unique to the Los Angeles–Long Beach area, such as unrelated shifts in industrial activity or weather patterns, that could independently influence local air quality.

Figure 7 visualizes monitor locations across port regions. Red markers represent Zone I monitors, while blue markers denote Zone II sites.[9]

Figure 7: AQI Monitor Local Sites



Note: Each polygon depicts a port area. Red sites represent zone I monitors. Blue sites represent zone II monitors.

I estimate the policy's effect on local air emissions using the following difference-

[9]Distances are computed using the Vincenty formula, which accounts for the Earth's ellipsoidal shape.

in-differences specification:

$$Y_{ipt} = \alpha + \gamma_1 T_p + \gamma_2 D_t + \gamma_3 (T_p \times D_t) + \varepsilon_{ipt}, \tag{4}$$

where Y_{ipt} is the pollution concentration recorded at monitor i, in port region p, on day t. The indicator T_p equals 1 for treated sites (Zone I monitors within 25 miles of the San Pedro Bay complex). D_t equals 1 for post-policy dates (Nov 11, 2021 onward). The coefficient γ_3 captures the average treatment effect on local pollution following the queuing policy.

Using particulate matter (PM) measures of pollutant concentrates, I find evidence of broad increases in emissions across monitors adjacent to the port area, relative to the outer zone of monitors (Table 7). PM_{10} emissions rose by a 25.8 percent and $PM_{2.5}$ rose by 5.5%. These results suggest a worsening in ambient air quality near the port despite reduced vessel idling. Sulfur dioxide (SO_2), on the contrary, declined slightly, although the estimate is statistically insignificant. This finding is notable, as SO_2 emissions are more directly attributable to maritime fuel combustion than particulate matter. The muted SO_2 response is consistent with earlier evidence of reduced emissions during the queuing phase, and may indicate that port-level pollution increases were driven by auxiliary sources of local economic activity rather than vessel operations alone.

Table 7: Difference-in-Difference, Control: San Pedro Bay, Zone-II

Dep. Variable:	PM_{10} (1)	$PM_{10-2.5}$ (2)	$PM_{2.5}$ (3)	SO2 (4)
Post–Period	-0.1898*	0.2919	-0.3486	0.3764*
	(0.0160)	(0.0582)	(0.2103)	(0.0311)
Treated	-0.3151***	-0.5804***	0.0032	-0.4552*
	(0.0018)	(0.0035)	(0.0014)	(0.0370)
DiD	0.2302**	0.1582**	0.0541*	-0.0966
	(0.0052)	(0.0070)	(0.0045)	(0.0349)
Day FE	✓	✓	✓	✓
Year–Month FE	✓	✓	✓	✓
Observations	6,949	1,303	14,471	3,853
R^2	0.22	0.40	0.25	0.19

Note: ***: 0.01, **: 0.05, *: 0.1. Standard-errors are robust to clustering by monitor zone. Each observation is a distinct day-monitor-port emission type reading. 'Post-Period' is equal to 1 for dates November 11th 2021 to October 30th 2022. 'Treatment' is equal to 1 for air pollutant concentration monitors within a 25-mile radius (Zone I) of the centroid of the San Pedro Bay port complex. The relevant control group consists of monitors within 25-50 miles of the same reference point (Zone II).

Referring to particulate matter emissions in Table 8, port-to-port difference-in-difference comparisons yield further evidence of a statistically significant rise in

Table 8: Difference-in-Difference, Control: Seattle/Oakland, Zone-I

Dep. Variable:	PM_{10} (1)	$PM_{10-2.5}$ (2)	$PM_{2.5}$ (3)	SO2 (4)
Post–Period	0.0164	-0.3332	0.4302	0.1943
	(0.2726)	(0.2562)	(0.3694)	(0.1447)
Treated	0.5940	1.426***	0.5539**	-0.2624**
	(0.2523)	(0.0051)	(0.1093)	(0.0510)
DiD	0.2863***	0.9336***	0.0107	-0.3240*
	(0.0264)	(0.0040)	(0.0113)	(0.1001)
Day FE	✓	✓	✓	✓
Year–Month FE	✓	✓	✓	✓
Observations	3,330	925	27,184	8,802
R^2	0.38	0.71	0.22	0.07

Note: ***: 0.01, **: 0.05, *: 0.1. Standard-errors are robust to clustering by monitor zone. Each observation is a distinct day-monitor-port emission type reading. 'Post-Period' is equal to 1 for dates November 11th 2021 to October 30th 2022. 'Treatment' is equal to 1 for air pollutant concentration monitors within a 25-mile radius (Zone I) of the centroid of the San Pedro Bay port complex. The relevant control group consists of monitors within 25 miles of the Port of Seattle and the Port of Oakland.

emissions upon the introduction of the new port queuing system. Notable deviations from the zone-based results listed in Table 7 include a near doubling of particulate matter between 2.5 and 10 micrometers in diameter. Additionally, a somewhat significant decline in sulfur dioxide is detected.[10]

Considering both sets of results, these findings suggest that while the queuing reform curbed emissions from individual vessels, aggregate pollution levels near San Pedro Bay increased following the policy's introduction. The rise in particulate matter near the port, despite muted changes in shipping-related sulfur emissions, hints at a broader intensification of local economic activity. This raises the possibility that, although the policy improved efficiency at the vessel level, the commercial appeal of greater queuing certainty may have also stimulated growth in port throughput. The next section investigates this commercial response, focusing on changes in port traffic volumes and their implications for local and regional environmental outcomes.

4.6. Commercial Port Activity

Although the ETA-based queue system improved the carbon efficiency of individual vessel voyages, increased scheduling certainty yielded offsetting behavioral responses. For example, should guaranteed queue positions be offered at a given port, this may present a better fit for 'just-in-time' production processes that many firms rely upon.

[10]See Appendix B3 for mirrored estimates with respect to carbon monoxide (CO), nitrogen dioxide (NO2), nitrogen oxides (NOx), and ozone gases.

This increased reliability diverted additional maritime commerce toward Los Angeles and Long Beach relative to other West Coast ports.

If the resulting growth in cargo throughput outpaces reductions in per-vessel emissions, the policy may generate a net rise in aggregate port-related pollution. To assess this possibility, I estimate difference-in-differences regressions comparing trade outcomes at San Pedro Bay to those observed at similar West Coast ports, before and after the policy's implementation.

Table 9: Difference-in-Difference, Commercial Activity

Dep. Variable:	Trade (USD) (1)	Trade (KG) (2)	Loaded Containers (3)	Total Containers (4)
Post–Period	-0.1077	-0.1662	-0.2055***	-0.2146***
	(0.1596)	(0.1164)	(0.0459)	(0.0560)
Treatment	1.019***	0.7442***	1.041***	1.126***
	(0.0392)	(0.0312)	(0.0124)	(0.0123)
DiD	0.0864	0.1310*	0.1575***	0.2192***
	(0.0849)	(0.0674)	(0.0249)	(0.0253)
Month-Year FE	✓	✓	✓	✓
Observations	600	600	600	600
R^2	0.62	0.59	0.95	0.96

Note: ***: 0.01, **: 0.05, *: 0.1. White Standard-errors, robust to the presence of heteroskedasticity. Each observation is a year-month of containerized trade outcomes at the port level between January 2012 and June 2024. 'Post-Period' is equal to 1 for dates after November 2021. 'Treatment' is equal to 1 for ports of San Pedro Bay. The relevant control group consists of the ports of Oakland, Seattle, and Tacoma. Dependent variables are in log-form. 'Trade (USD)' represents the real value of containerized exports and imports, deflated using the St Louis FED's Consumer Price Index for All Urban Consumers: All Items Less Food and Energy in U.S. City Average. 'Trade (KG)' represents the total kilogram weight of containerized imports and exports. 'Loaded Containers' uses bilateral loaded container traffic flows reported directly by individual ports as a measure of market share/throughput. 'Total Containers' includes bilateral port flows of both loaded and empty containers.

Table 9 shows that commercial activity at San Pedro Bay rose significantly relative to control ports following the queuing reform. The increase ranges from roughly 8% for trade value to over 21% for total container volumes, with the largest relative growth observed in empty container movement. Even when restricting the sample to the COVID-era window surrounding the reform, results are consistent and suggestive of a structural increase in throughput.

Although gains point to efficiency improvements, they also suggest an intensification of activity that could counteract local environmental benefits.

5. Welfare Analysis

This section quantifies the local welfare consequences of the queuing reform at San Pedro Bay, focusing exclusively on emissions experienced in the vicinity of the ports of Los Angeles and Long Beach. Two distinct effects are assessed: (i) a reduction in queuing emissions per international vessel voyage following the introduction of

ETA-based scheduling, and (ii) an overall increase in port emissions attributable to diverted trade flows from competing West Coast ports.

5.1. Monetized Effects of Queuing Emissions

To monetize the reduction in carbon dioxide emissions, I apply a local social cost of carbon (SCC) of $185 per metric ton of CO_2, based on the damage functions and discounting framework developed by Rennert et al. (2022). Although the SCC is often interpreted as a measure of global damages, this value is increasingly used to reflect marginal domestic harm under U.S. policy analysis. It integrates recent advances in damage modeling, socioeconomic forecasting, and discounting, and is consistent with the EPA's revised 2022 valuation of $190 per ton (EPA, 2022).[11]

Referring to Table 5, the policy reduced emissions per voyage by approximately 26.3 percent. Letting $\widehat{\tau}$ denote the proportional emissions reduction, the counterfactual emissions in the absence of treatment are computed as

$$\widehat{E}_{\text{counterfactual}} = \frac{\sum_{i \in \text{treated, post}} E_i}{1 + \widehat{\tau}}, \quad \widehat{E}_{\text{reduction}} = \widehat{E}_{\text{counterfactual}} - \sum_{i \in \text{treated, post}} E_i.$$

where E_i represents emissions across the queuing stage of transit for each vessel i, summed across international transits during the post-reform period.[12] This amounts to taking the sum of emissions across all treated vessel-voyages in the post-period, servicing international transportation, and scaling this sum by the inverse of the emissions reduction rate, $\exp(-0.3046)$.

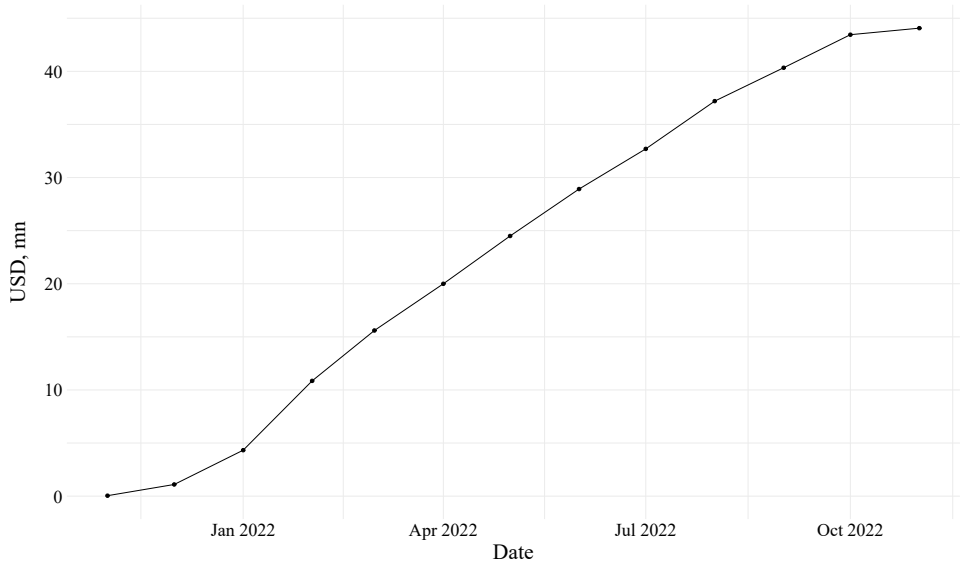
I estimate a reduction of $238,199$ metric tons of CO_2 from November 2021 through 2022. Using a social cost of $185 per ton of carbon, the monetized benefits of the queuing system change on per-vessel emissions accumulate to 44.1mn USD (Figure 8).

To put this in scale, the first phase of the Ocean-Going Vessel At-Berth Regulation, implemented across multiple Californian ports to lower docked vessel emissions, yielded savings of $558mn USD in medical costs per year (Gillingham and Huang, 2021). Given the narrower extent to which this queue system was adopted, and its low cost of implementation, a broader implementation of an ETA-based approach may help further the aims of the California Air Resources Board. However, due to

[11] This estimate represents a substantial upward revision from prior SCC values—such as the Interagency Working Group's (IWG) central estimate of $51 per ton or Nordhaus's earlier DICE-based estimates in the $31–$50 range (Nordhaus, 2017; IWG, 2021).

[12] Given that voyage emissions occur outside of US waters, deep at sea, it is arguable that social costs of carbon are significantly lower.

Figure 8: Cumulative social benefit of per-vessel emission reduction



Note: Based on author's calculations, specific to the queuing stage of vessel transit.

the isolated manner in which the ETA-based system was introduced, San Pedro Bay effectively triggered trade diversion from other West Coast ports. This contributed to an overall increase in emissions across multiple types of pollutants.

5.2. Monetized Emissions Effects of Queue System

To construct damage estimates, I use data on emission inventories of Los Angeles and Long Beach ports, estimates of proportional changes in $PM_{2.5}$, NO_x, and SO_2, and the AP3 integrated assessment model, featured in Clay et al. (2019). The AP3 model is an air pollution model that estimates changes in county-level air pollution based on changes in emissions. Peer-reviewed concentration-response functions are applied, based on calculated exposures and US census data, which enables exposures to be converted to physical effects. Most of the marginal changes in damages yielded by AP3 are due to increased mortality and the social cost of carbon.

Upon running the model using its 2014 configuration, it provides marginal damages of pollutants emitted by ground level, low stack and medium sources for all 3,109 counties included. Ground level sources include road dust, fugitive emissions, vehicles. Low stack sources would consist of small boilers, heating, ventilation, air conditioning, and port equipment with vertical ventillation in the 5-10 meter range. Medium stacks are attributed to industrial stacks and larger exhausts, normally 10-30 meters in vertical height. Given my suggestion of greater commercial acitivty at the port, consisting of greater rates of container restacking, forklift use, crane

movements, and intermodal transport exchange (e.g. trucks and rail), I examine the implications of relying on 'low' and 'ground' level emissions.

I detect air quality changes across monitors within 25 miles of the San Pedro Bay port complex. This set of treated monitors occupies two US counties, Los Angeles and Orange County. I assign a rate of marginal damage for each emission type ($PM_{2.5}$, NO_X, and SO_2) based on a cross-county weighted average. Weights are determined by each county's share of total landmass featured within the 25 mile centroid radius. To estimate the environmental cost of this policy, interact a marginal damages (2014 USD per ton) with the change in total emissions tonnage.

Ideally, I would use the total change in emissions in the 25 mile radius surrounding the port centroid. However, air quality monitors dotted around this space only report ambient pollution rates, air quality, rather than total emission inventory for the region. I elect to use total volume of 2022 port emissions as the next best alternative, sourced from each port's respective annual 'Inventory of Air Emissions' report. These inventories include contributions by ocean-going vessels, harbor craft, cargo handling equipment, locomotives, and heavy-duty vehicles. The estimated monetized environmental damages that this system yields, due to inadvertently attracting competitor ports' traffic, should therefore be considered a baseline estimate. It does not account for added commercial traffic travelling within the 25 mile radius of the treatment area, that likely increases associated environmental damages further, through air quality degradation.

Table 10 displays the key metrics I use to determine estimated environmental damages associated with the introduction of ETA-based queuing in San Pedro Bay.

Table 10: Queue System Damages - Key Parameters

Parameter	Year	$PM_{2.5}$	NO_X	SO_2
MD, Area, USD per short ton	2014	905,736.7	153,412.9	413,502.9
MD, Low Stack, USD per short ton	2014	711,536.6	111,232.7	318,144.1
LA Port Em. Inventory, metric tons	2022	113	5,765	136
Long Beach Em. Inventory, metric tons	2022	157	7,686	252
Emission Change, $\Delta\hat{E}_{low}$, %	2022	0.011	0.119	-0.277
Emission Change, $\Delta\hat{E}_{high}$, %	2022	0.056	0.205	-0.092

Source: Marginal damages (MD) averages, using AP3 estimates, are based on the assumption of constant population density across the subsections of Los Angeles and Orange County considered. Los Angeles Inventory Of Air Emissions 2022, Table ES.2 and Long Beach 2022 Air Emissions Inventory, Table ES.2. High and low point estimates of $PM_{2.5}$ and SO_2 emission changes stem from columns (3) and (4) of Tables 7 and 8, respectively. NO_X estimates are presented in Appendix B3. All six coefficients stem from log-level regressions and are interpretable only upon being fed into $\exp(\hat{\beta}) - 1$.

The resulting environmental costs are calculated by interacting these marginal damage rates with the estimated tonnage changes. Area-based damages range between $218–474 million, while low-stack estimates range from $155–344 million (all in 2022 USD).[13] These costs represent a lower bound, as they exclude inland freight and secondary pollution associated with higher throughput beyond the port zone. Although the magnitude of local damages is nontrivial, they remain smaller than the $558 million in annual savings attributed to the first-phase of California's At-Berth Regulation (Gillingham and Huang, 2021). As discussed in the next section, queuing reform may yield offsetting economic benefits via enhanced scheduling certainty for shippers.

5.3. Net Impact and Distributional Considerations

A complete welfare assessment of the queuing reform would require structural modeling of trade diversion effects, supply chain reoptimization, and resulting localized pollution impacts – all of which lie beyond the scope of this paper. Instead, I offer a partial equilibrium view that emphasizes the trade-offs between environmental externalities and commercial throughput gains at San Pedro Bay.

Shapiro (2016) supports the view that greater trade and transportation flows yield trade-related welfare gains, undermined by associated emission-related losses of higher transport service volume. From a global perspective, trade gains outweigh emission losses by a significant margin. Supposing US ports broadly adopt an ETA-based queuing system, this may limit within-country trade diversion, while potentially attracting trade flows from other countries. Reduced idling time and greater certainty surrounding port admittances raises the effective supply of global shipping capacity, adding downward pressure to prevailing global freight rates. Furthermore, given that per-vessel emissions would decline, this would mitigate the countervailing welfare losses associated with transport service volume growing. The associated welfare gain for the overall US population is therefore likely positive, however, the welfare effect of a local populace bearing the brunt of this transport service influx is unclear. Residents of Los Angeles and Orange Counties would still bear a disproportionate share of the damages, despite reaping only diffuse or indirect economic benefits. Under an isolated introduction of ETA-based queuing, I estimate emission-related welfare losses ranging between $155-474mn in 2022.[14]

[13] I adjusted the list AP3 values, expressed in 2014 USD per ton, for inflation using the CPI-U for all items excluding food and energy.

[14] Census tract data for 2022 reports an estimated population of 7.5 million for the 25 mile radius surrounding the San Pedro Bay ports. This implies a cost of additional port emissions ranging between 20-62 USD per capita.

6. Conclusion

This paper evaluates the environmental consequences of a novel queuing system change introduced at the Ports of Los Angeles and Long Beach in late 2021. By assigning vessels a queue position at their point of departure, based on estimated time of arrival, rather than upon arrival, the policy altered longstanding operational incentives, enabling ships to slow-steam and synchronize more efficiently with berth availability. Through the use of high-frequency vessel tracking data, port call records, and emissions estimates, I document that the reform substantially reduced offshore idling and emissions intensity.

Average queuing time fell by 33.3 percent, local emissions per vessel declined by 26.3 percent, and voyage emissions dropped by 9.5 percent. These results show that logistical coordination alone can drive measurable decarbonization in maritime freight, without requiring capital-intensive retrofitting or broad regulatory mandates. While voyage speed reductions proved temporary, dissipating within a year, gains in queuing efficiency persisted throughout the sample window. Although it represents a narrow share of the geography of each voyage, the queuing stage accounts for 10–50 percent of the total transit time and 5–25 percent of emissions, depending on the length of the voyage. Upon controlling for both reduced idling and slower steaming, I estimate that the policy lowered international voyage emissions, per vessel, by 10 percent and emissions per nautical mile by 13 percent.

Despite these per-vessel improvements, I show that air quality near the ports deteriorated. EPA monitor data reveal a post-policy increase in local pollution levels relative to other West Coast port regions. I attribute this to increased commercial throughput at San Pedro Bay, which saw a post-policy relative rise of 14-24.5 percent, depending on the trade volume metric. These results underscore a key distinction. Operational improvements can reduce emissions intensity, but not necessarily total emissions, particularly when they increase a port's attractiveness and traffic volume. In the case of San Pedro Bay, AP3 model estimates suggest environmental damages, mostly linked to increased mortality risk, in the range of $155-474mn for the year of 2022.

These findings offer both encouragement and caution. They demonstrate that modest reforms to port logistics can yield substantial efficiency and emissions gains. However, they also underscore the backfiring risks of localized interventions, especially when those reforms amplify commercial activity in highly populated areas. As maritime regulators seek to decarbonize global shipping, queuing reform represents

a cost-effective, scalable strategy, best implemented as part of a broader package of emissions and exposure controls.

Future research should assess the applicability of ETA-based queuing reforms at smaller or less congested ports, where idling is less pronounced and gains may be more limited. Moreover, further attention is needed to quantify the welfare trade-offs between the indirect commercial gains and localized pollution burdens of greater port traffic in densely populated port communities. While queuing reform enhances operational efficiency and port competitiveness, its net welfare impact hinges on how commercial gains are distributed relative to the spatial incidence of pollution exposure.

References

Auffhammer, M. and R. Kellogg (2011). Clearing the Air? The Effects of Gasoline Content Regulation on Air Quality. *American Economic Review 101*(6), 2687–2722.

Bai, C., Y. Li, B. Liu, Z. Zhang, and P. Wu (2020). Gaseous Emissions from a Seagoing Ship under Different Operating Conditions in the Coastal Region of China. *Atmosphere 11*(3).

Boarnet, M. G., X. Wang, and D. Houston (2017). Can new light rail reduce personal vehicle carbon emissions? a before-after, experimental-control evaluation in los angeles. *Journal of Regional Science 57*(3), 523–539.

Brancaccio, G., M. Kalouptsidi, and T. Papageorgiou (2020). Geography, transportation, and endogenous trade costs. *Econometrica 88*(2), 657–691.

Capaldo, K., J. J. Corbett, P. Kasibhatla, P. Fischbeck, and S. N. Pandis (1999). Effects of ship emissions on sulphur cycling and radiative climate forcing over the ocean. *Nature 400*(6746), 743–746.

Clay, K., A. Jha, N. Muller, and R. Walsh (2019). External Costs of Transporting Petroleum Products: Evidence from Shipments of Crude Oil from North Dakota by Pipelines and Rail. *The Energy Journal 40*(1), pp. 55–72.

Corbett, J. J., H. Wang, and J. J. Winebrake (2009). The effectiveness and costs of speed reductions on emissions from international shipping. *Transportation Research Part D: Transport and Environment 14*(8), 593–598.

Corbett, J. J., J. J. Winebrake, E. H. Green, P. Kasibhatla, V. Eyring, and A. Lauer (2007). Mortality from Ship Emissions: A Global Assessment. *Environmental Science and Technology 41*(24), 8512–8518. PMID: 18200887.

Cristea, A., D. Hummels, L. Puzzello, and M. Avetisyan (2013). Trade and the greenhouse gas emissions from international freight transport. *Journal of Environmental Economics and Management 65*(1), 153–173.

Czermański, E., G. T. Cirella, A. Oniszczuk-Jastrzabek, B. Pawłowska, and T. Notteboom (2021). An Energy Consumption Approach to Estimate Air Emission Reductions in Container Shipping. *Energies 14*(2).

Davies, R. and T. Jeppesen (2015). Export mode, firm heterogeneity, and source country characteristics. *Review of World Economics (Weltwirtschaftliches Archiv) 151*(2), 169–195.

Economides, P. (2024). Unconventional Protectionism in Containerized Shipping. In *Working Papers Set*.

EPA (2022). Report on the social cost of greenhouse gases: Estimates incorporating recent scientific advances. Technical report, U.S. Environmental Protection Agency.

Ganapati, S. and W. F. Wong (2023). How Far Goods Travel: Global Transport and Supply Chains from 1965–2020. *Journal of Economic Perspectives 37*(3), 3–30.

Gillingham, K. and P. Huang (2021). Racial Disparities in the Health Effects from Air Pollution: Evidence from Ports. NBER Working Papers 29108, National Bureau of Economic Research, Inc.

Gupta, A., S. Van Nieuwerburgh, and C. Kontokosta (2020). Take the Q Train: Value Capture of Public Infrastructure Projects. Working Paper 26789, National Bureau of Economic Research.

Hansen-Lewis, J. and M. M. Marcus (2022). Uncharted waters: Effects of maritime emission regulation. Technical report, National Bureau of Economic Research.

Heiland, I., A. Moxnes, K. H. Ulltveit-Moe, and Y. Zi (2019). Trade From Space: Shipping Networks and The Global Implications of Local Shocks. CEPR Discussion Papers 14193, C.E.P.R. Discussion Papers.

Hulskotte, J. and H. Denier van der Gon (2010). Fuel consumption and associated emissions from seagoing ships at berth derived from an on-board survey. *Atmospheric Environment 44*(9), 1229–1236.

IMO (2021). Fourth Greenhouse Gas Study 2020. Full report, International Maritime Organization.

IWG (2021). Technical Support Document: Social Cost of Carbon, Methane, and Nitrous Oxide. Technical report, Interagency Working Group on Social Cost of Greenhouse Gases, U.S. Government.

Jalkanen, J.-P., L. Johansson, J. Kukkonen, A. Brink, J. Kalli, and T. Stipa (2012). Extension of an assessment model of ship traffic exhaust emissions for particulate

matter and carbon monoxide. *Atmospheric Chemistry and Physics 12*(5), 2641–2659.

Ju, Y. and C. A. Hargreaves (2021). The impact of shipping co2 emissions from marine traffic in western singapore straits during covid-19. *Science of The Total Environment 789*, 148063.

Kinney, P. L., M. G. Gichuru, N. Volavka-Close, N. Ngo, P. K. Ndiba, A. Law, A. Gachanja, S. M. Gaita, S. N. Chillrud, and E. Sclar (2011). Traffic impacts on PM2.5 air quality in Nairobi, Kenya. *Environmental Science & Policy 14*(4), 369–378.

Klotz, R. and J. Berazneva (2022). Local Standards, Behavioral Adjustments, and Welfare: Evaluating California's Ocean-Going Vessel Fuel Rule. *Journal of the Association of Environmental and Resource Economists 9*(3), 383 – 424.

Linden, L. and J. E. Rockoff (2008). Estimates of the Impact of Crime Risk on Property Values from Megan's Laws. *American Economic Review 98*(3), 1103–27.

Liu, H., M. Fu, X. Jin, Y. Shang, D. Shindell, G. Faluvegi, C. Shindell, and K. He (2016). Health and climate impacts of ocean-going vessels in East Asia. *Nature Climate Change 6*(11), 1037–1041.

Ludwig, P. (2025). Can Unilateral Policy Decarbonize Maritime Trade? CESifo Working Paper Series 11712, CESifo.

Lugovskyy, V., A. Skiba, and D. Terner (2023). Unintended Consequences of Environmental Regulation of Maritime Shipping: Carbon Leakage to Air Shipping. In *SSRN Electronic Journal*.

McDermott, G. R., K. C. Meng, G. G. McDonald, and C. J. Costello (2019). The Blue Paradox: Preemptive overfishing in marine reserves. *Proceedings of the National Academy of Sciences 116*(12), 5319–5325.

Mitchell, R. C. and R. Carson (1986). Property Rights, Protest, and the Siting of Hazardous Waste Facilities. *American Economic Review 76*(2), 285–90.

Molina, R., J. C. Villaseñor-Derbez, G. McDonald, and G. McDermott (2024). Dangerous Waters: The Economic Toll of Piracy on Maritime Shipping. CESifo Working Paper Series 11077, CESifo.

Morehouse, J. M. and E. A. Rubin (2021). Downwind and Out: The Strategic Dispersion of Power Plants and their Pollution. In *SSRN Electronic Journal*.

Ngo, N. S., M. Gatari, B. Yan, S. N. Chillrud, K. Bouhamam, and P. L. Kinney (2015). Occupational exposure to roadway emissions and inside informal settlements in sub-Saharan Africa: A pilot study in Nairobi, Kenya. *Atmospheric Environment 111*, 179–184.

Nordhaus, W. D. (2017). Revisiting the social cost of carbon. *Proceedings of the National Academy of Sciences 114*(7), 1518–1523.

Prochazka, V., R. Adland, and F.-C. Wolff (2019). Contracting decisions in the crude oil transportation market: Evidence from fixtures matched with AIS data. *Transportation Research Part A: Policy and Practice 130*(C), 37–53.

Rennert, K., F. Errickson, B. Prest, L. Rennels, R. Newell, W. Pizer, C. Kingdon, J. Wingenroth, R. Cooke, B. Parthum, D. Smith, K. Cromar, D. Diaz, F. Moore, U. Müller, R. Plevin, A. Raftery, H. Ševčíková, H. Sheets, J. Stock, T. Tan, M. Watson, T. Wong, and D. Anthoff (2022). Comprehensive evidence implies a higher social cost of CO2. *Nature 610*(7933), 687–692.

Rivera, N. (2021). Air quality warnings and temporary driving bans: Evidence from air pollution, car trips, and mass-transit ridership in Santiago. *Journal of Environmental Economics and Management 108*(C), S0095069621000371.

Rodrigue, J.-P. (2020, May). *The Geography of Transport Systems*. Fifth edition. — Abingdon, Oxon ; New York, NY : Routledge, 2020.: Routledge.

Schwarzkopf, D. A., R. Petrik, V. Matthias, M. Quante, E. Majamäki, and J.-P. Jalkanen (2021). A ship emission modeling system with scenario capabilities. *Atmospheric Environment: X 12*, 100132.

Scott, T. M. and F. Mayer (2023). International Trade, Noise Pollution, and Killer Whales. NBER Working Papers 31390, National Bureau of Economic Research, Inc.

Shapiro, J. (2016). Trade Costs, CO2, and the Environment. *American Economic Journal: Economic Policy 8*(4), 220–54.

Tumbarello, P., S. Arslanalp, and M. Marini (2019). Big Data on Vessel Traffic: Nowcasting Trade Flows in Real Time. IMF Working Papers 2019/275, International Monetary Fund.

Walsh, C. and A. Bows (2012). Size matters: Exploring the importance of vessel characteristics to inform estimates of shipping emissions. *Applied Energy 98*(C), 128–137.

Wang, S., Q. Meng, and M. G. Bell (2013). Liner ship route capacity utilization estimation with a bounded polyhedral container shipment demand pattern. *Transportation Research Part B: Methodological 47*, 57–76.

Wong, W. F. (2022). The Round Trip Effect: Endogenous Transport Costs and International Trade. *American Economic Journal: Applied Economics 14*(4), 127–66.

Wong, W. F. and S. Fuchs (2022). Multimodal Transport Networks. FRB Atlanta Working Paper 2022-13, Federal Reserve Bank of Atlanta.

Zhang, Y., S. D. Eastham, A. K. Lau, J. C. Fung, and N. E. Selin (2021, aug). Global air quality and health impacts of domestic and international shipping. *Environmental Research Letters 16*(8), 084055.

Zou, E. Y. (2021). Unwatched Pollution: The Effect of Intermittent Monitoring on Air Quality. *American Economic Review 111*(7), 2101–26.

A Data Appendix

A1. Vessel Traffic

I construct voyage-level data on emissions by combining vessel position records with port call data. These measures are developed through multiple stages of cleaning and alignment using high-frequency vessel tracking data provided by MarineCadastre (MC) and port call data provided by MarineTraffic (MT).

Port Statistical Areas

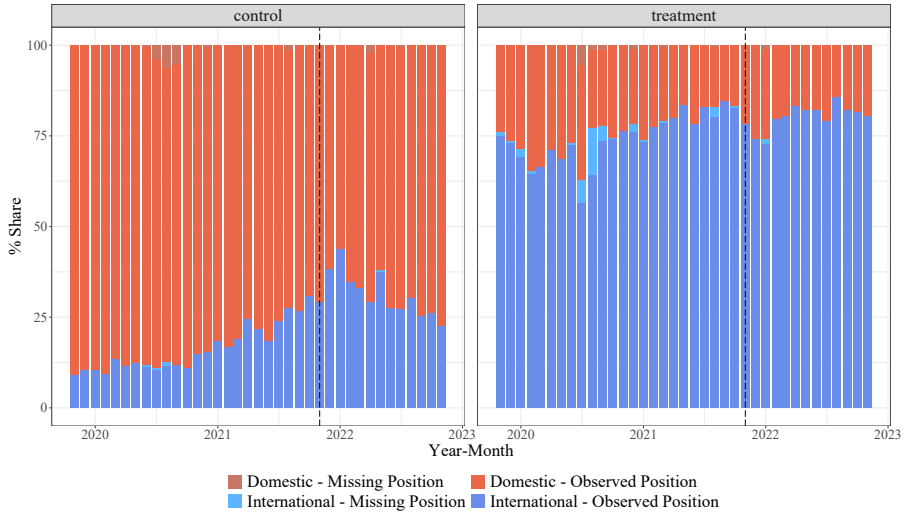
I identify major container ports based on Panjiva records of twenty-foot equivalent unit (TEU) throughput.[15] Geospatial boundaries for these ports – referred to as Port Statistical Areas – are obtained from the U.S. Army Corps of Engineers (USACE). These polygons are used to identify the precise moment a vessel enters or exits a West Coast port. I treat the Ports of Los Angeles and Long Beach as a single port complex, assigning them a shared centroid for constructing radius-based treatment zones.

Matching MarineTraffic (MT) and MarineCadastre (MC)

MarineTraffic (MT) provides global port call records, detailing each vessel's departure timestamp, destination, and estimated travel distance. However, these data do not distinguish between the voyage and queuing segments of transit. In many instances, vessels idle just offshore for extended periods, which can bias voyage duration and speed estimates downward. To isolate the voyage segment, I match each MT departure to the first MC AIS ping in U.S. waters. MC records vessel position data at one-minute intervals, which enables near-exact identification of this arrival point. Each IMO-identified vessel is matched based on the time window between port departure and subsequent arrival at a U.S. West Coast port. This allows me to compute the speed and distance of the voyage segment. The queuing segment is defined as the interval between a US water arrival point and the moment of port admittance. Port admittance is defined as the timestamp when a vessel crosses into the relevant USACE port polygon and comes to a complete stop in a berthing area. Together, these three events − departure, offshore arrival, and berthing − allow me to reconstruct the full transit path of each vessel. In Figure A1, I discern which transits in US waters represent international journeys − the key focus of this study.

[15] See https://www.logisticsmgmt.com/article/top_30_u.s._ports_big_ports_got_bigger_in_2020

Figure A1: Match Status by Origin and Group



Distances between departure and offshore arrival are computed using Vincenty ellipsoid geodesic methods to account for Earth's curvature. Queuing distances are calculated using the Haversine formula applied to sequential AIS pings.

After assembling the panel of West Coast-bound voyages, I merge in vessel registry data from VesselTracking.net, which reports TEU capacity and build year. To ensure comparability, I restrict attention to IMO-certified containerships with verified TEU capacities in the VesselTracking registry. Vessels with military, recreational, or non-container cargo designations are excluded. A small subset of port call vessels are not detected in US waters within their respective prescribed time windows. I label these cases as "missing". The overall rate of missingness is below 1 percent of the MT sample, with a notable increase in July 2020, concentrated around California port calls.

To address extreme outliers in voyage speed, I follow Davies and Jeppesen (2015), defining outliers as values outside a range bounded by the 25th percentile minus three times the interquartile range (IQR) and the 75th percentile plus three times the IQR of observed average speeds. After removing outliers, the final dataset includes 10,035 voyages from 1,061 distinct containerships.

Many of these voyages involve vessels making multiple port calls at nearby locations on the West Coast. For my second set of analysis, I restrict attention to international voyages by discarding transits between US, Canadian, and Mexican ports. This restriction yields a sample of 5,671 international port visits by 990 distinct vessels.

The potential for strategic routing responses by vessel operators in reaction to the policy presents an identification concern. To circumvent queuing restrictions, operators may redirect inbound vessels to initially arrive at untreated ports, subsequently proceeding to treated destinations under reduced policy exposure. To address this, I construct a balanced panel restricted to vessels that consistently serviced the same treated ports in both the pre- and post-policy periods. I exclude "switcher" vessels that changed their initial US port of arrival, "entrant" vessels that first appear only after the policy, and "exit" vessels that cease West Coast activity post-policy.

This balanced sample forms the basis for my main results and consists of 2,354 port visits by 301 distinct vessels with uninterrupted service to treated ports across both periods. Given the nature of commercial shipping, where route assignments are often governed by long-term capacity optimization rather than short-term operational discretion, many switchers, entrants, and exits likely reflect routine network adjustments rather than policy-induced selection. This interpretation is supported by the robustness of estimated effects: regressions that include the full international transit sample – including all route-changing vessels – yield results that are nearly indistinguishable from those based on the balanced panel.

A2. Fuel Consumption Function

To estimate vessel-level daily fuel consumption, I recover functional relationships between vessel speed (knots) and fuel usage (tons/day) by digitizing the curves displayed in Figure A2, sourced from Rodrigue (2020).[16] These curves report fuel consumption across five container ship classes, categorized by TEU capacity ranges. Using a digital extraction tool, I convert each curve into coordinate point data and assign TEU bin midpoints to define ship size. The 10,000+ TEU category is omitted from estimation due to the absence of a meaningful midpoint. I construct a grid of 1,000 equidistant speed points ranging from 0 to 25 knots. For each speed value, I compute predicted fuel consumption using the digitized functions, generating a dataset of speed (X), TEU capacity (Z), and corresponding fuel consumption levels (Y). I then estimate the following bivariate polynomial regression model:

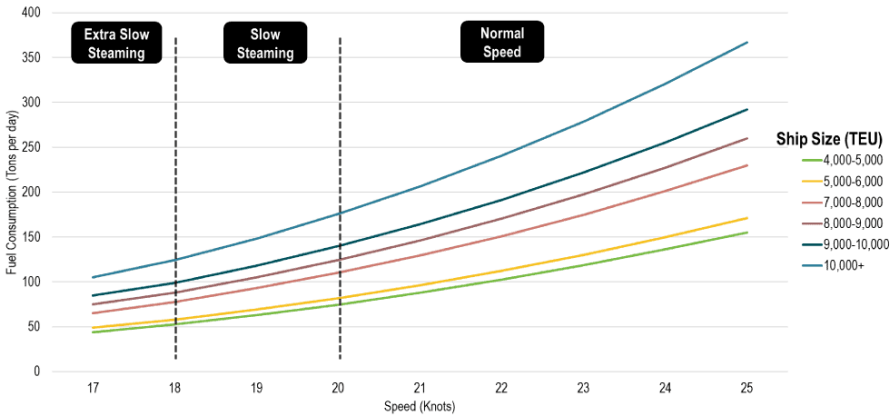
$$Y_i = \alpha + \beta_1 X_i + \beta_2 Z_i + \beta_3 X_i^2 + \beta_4 Z_i^2 + \beta_5 X_i \times Z_i + \beta_6 X_i^2 \times Z_i + \varepsilon_i. \tag{5}$$

The estimated coefficients $\{\hat{\alpha}, \hat{\beta}_1, \ldots, \hat{\beta}_6\}$ yield a flexible function for predicting

[16] I do not observe engine types across vessels necessary to use a naval engineering approach featured in Corbett et al. (2009) and Lugovskyy et al. (2023). Ship size suffices in applied studies of vessel emissions (Walsh and Bows, 2012).

daily fuel consumption as a function of vessel speed and TEU capacity. The resulting surface is convex in speed and exhibits a non-linear increase with vessel size, consistent with basic energy cost scaling principles in maritime transport.

Figure A2: Fuel Consumption by Speed and TEU Capacity



Source: Rodrigue (2020). The Geography of Transport Systems, Chapter 4, Transportation and Energy.

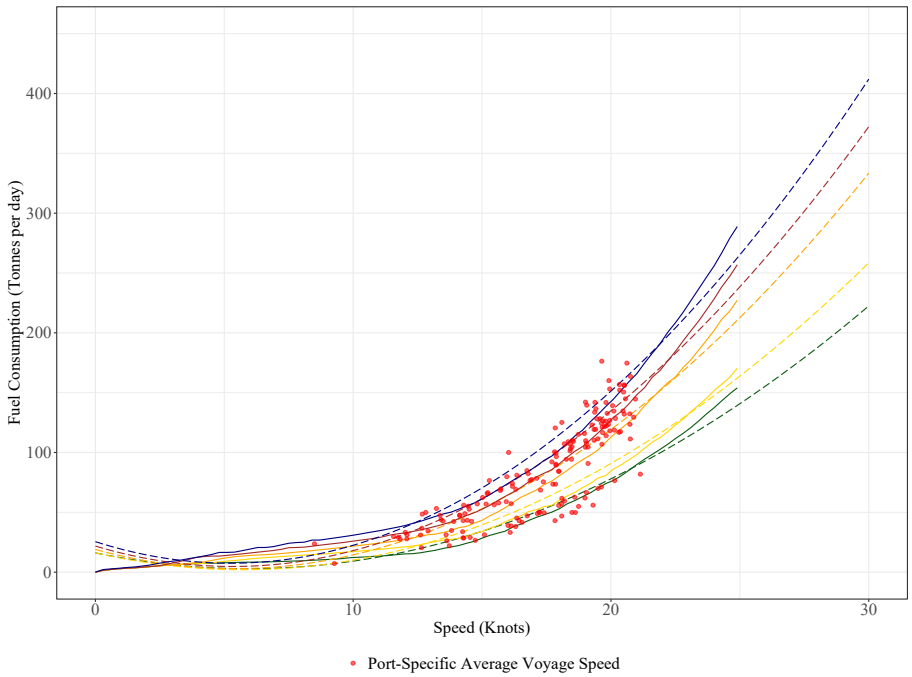
Figure A3 compares the fitted curves from Equation 5 (dashed lines) with the original digitized consumption functions (solid lines) across TEU capacity bins. The polynomial model provides a close approximation in the empirically relevant speed range of 10–25 knots, where most observed vessel operations occur. To reinforce this, I overlay port-specific average voyage speeds as red points. These fall predominantly within the region where interpolated and digitized functions tightly align, suggesting the model performs well over the support of the observed data. At slower speeds (e.g., < 10 knots), the fitted model diverges more significantly from source curves. In these regions, corresponding to low-speed maneuvering behavior, I supplement the analysis using external engineering estimates, as detailed in the next subsection.

A3. Queuing Emissions

To estimate queuing activity emissions, I apply an adjustment procedure for vessels operating at low or stationary speeds, which are not well captured by standard cruising-based fuel consumption functions. I follow the approach of Bai et al. (2020), who estimate emissions during the maneuvering, anchoring, and low-speed cruising phases using high-resolution data from port areas in coastal China. This study decomposes local vessel behavior into distinct speed stages and reports associated emission concentrations as vessels accelerate from stationary to maneuvering states.

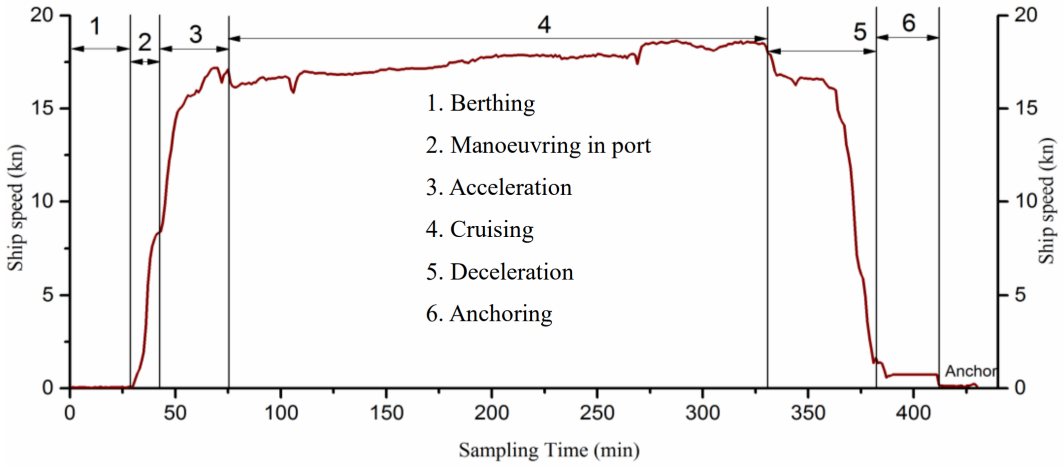
Figures A4 and A5 illustrate the distribution of vessel speeds by operational mode and the corresponding variation in gaseous emissions.

Figure A3: Fuel Consumption Function



Note: Dashed lines represent imputed functions with TEU fixed at the midpoint of ranges associated with solid line. Solid line functions were mapped using graph readers applied to figures featured in Rodrigue (2020). Solid red points correspond to port-specific average travel speeds of voyages destined for US West Coast ports.

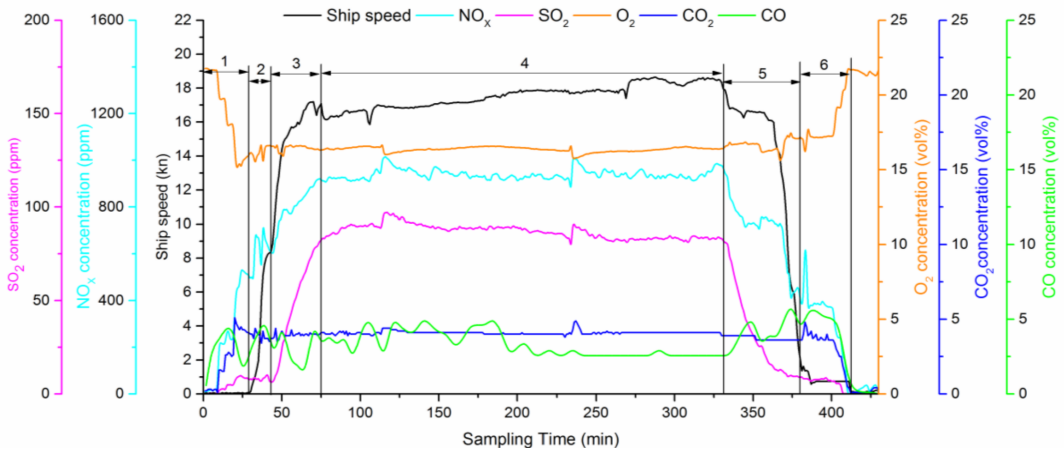
Figure A4: Speed by Stage



Source: Bai et al. (2020), Gaseous Emissions from a Seagoing Ship under Different Operating Conditions in the Coastal Region of China, Atmosphere, Vol. 11(3), pp 305.

For each vessel i located within US waters at time t, moving at speed S_{ipt}, and carrying capacity C_i, I calculate emissions between consecutive AIS pings t and $t' < t$ at one-minute resolution. Assuming compliance with IMO 2020 sulfur content limits, I apply fuel-based emissivity indices (in kg/ton of fuel) as featured in Table 2.

Figure A5: Emissions by Speed-Stage



Source: Bai et al. (2020), Gaseous Emissions from a Seagoing Ship under Different Operating Conditions in the Coastal Region of China, Atmosphere, Vol. 11(3), pp 305.

For each interval between AIS signals, I compute emissions in three steps:

If $S_{ipt} > 10$:

1. Estimate fuel consumption: $\Phi_{ipt} = \Phi(S_{ipt}, C_i)$ (tons/day)
2. Scale to emissions: $\Phi_{ipt} \cdot$ Emissivity Indices (kg/day)
3. Scale to time window:

$$\delta_{ipt} = \left(\frac{t - t'}{24}\right) \cdot \Phi_{ipt} \cdot \text{Emissivity Indices}$$

If $S_{ipt} \leq 10$, I fix fuel consumption at $\Phi(10, C_i)$ but apply an emissions scaling factor (ESF) to reflect reduced pollutant concentrations at lower speeds. This factor is estimated from Bai et al. (2020) using reported NO_X concentrations, which decrease non-linearly from 700 ppm at 10 knots to 450 ppm at 0 knots.

$$ESF(S_{ipt}) = 64.29 + 7.54 \cdot S_{ipt} - 0.40 \cdot S_{ipt}^2$$

Emissions during low-speed transits are therefore computed as:

$$\delta_{ipt} = \left(\frac{t - t'}{24}\right) \cdot \Phi(10, C_i) \cdot ESF(S_{ipt}) \cdot \text{Emissivity Indices}$$

For static berth activity, I recommend the use of a scaling factor proposed by Hulskotte and Denier van der Gon (2010) which receive frequent use in the maritime logistics literature (Jalkanen et al., 2012; Ju and Hargreaves, 2021; Schwarzkopf et al., 2021). This is a linear function of the gross tonnage of vessels times the hours

spent stationary (Table A1). For the purposes of this study, assessing voyage and queuing stages of transit, I do not include berthing activity in broader analysis.

Table A1: Estimate of Fuel Consumption by GT-Dwell Hours

Type of ship	Fuel Consumption Rate (kg fuel/1000 GT h)	Average hotelling time at berth (hours)
Oil Tankers	19.3	28
Chemical and other tankers	17.5	24
Bulk Carriers	2.4	52
Containers	5.0	21
General Cargo	5.4	25
Ferries and RoRo	6.9	24
Reefers	24.6	31
Other	9.2	46

Source: Hulskotte and Denier van der Gon (2010). Fuel Consumption and Associated Emissions from Seagoing Ships at Berth Derived from Onboard Survey, Atmospheric Environment, Vol. 44(9), pp 1229–1236.

This procedure yields estimates of vessel emissions during queuing, anchored, and maneuvering stages, disaggregated by pollutant type and vessel identity. These values are used to evaluate policy impacts on localized maritime emissions.

A4. Air Quality Monitoring and Wind Direction

To assess the localized impact of vessel emissions, I use air quality monitoring data from the U.S. Environmental Protection Agency (EPA), spatially restricted to counties adjacent to major West Coast container ports. Counties are assigned to specific ports based on geographic proximity and metropolitan integration, yielding three focal port groups: Los Angeles and Long Beach (LA+LB), Oakland, and Seattle. Each EPA monitoring site is geocoded using its latitude and longitude, and its distance to the centroid of the associated port polygon – defined via USACE Port Statistical Areas – is computed using Vincenty ellipsoid formulas to account for Earth's curvature.

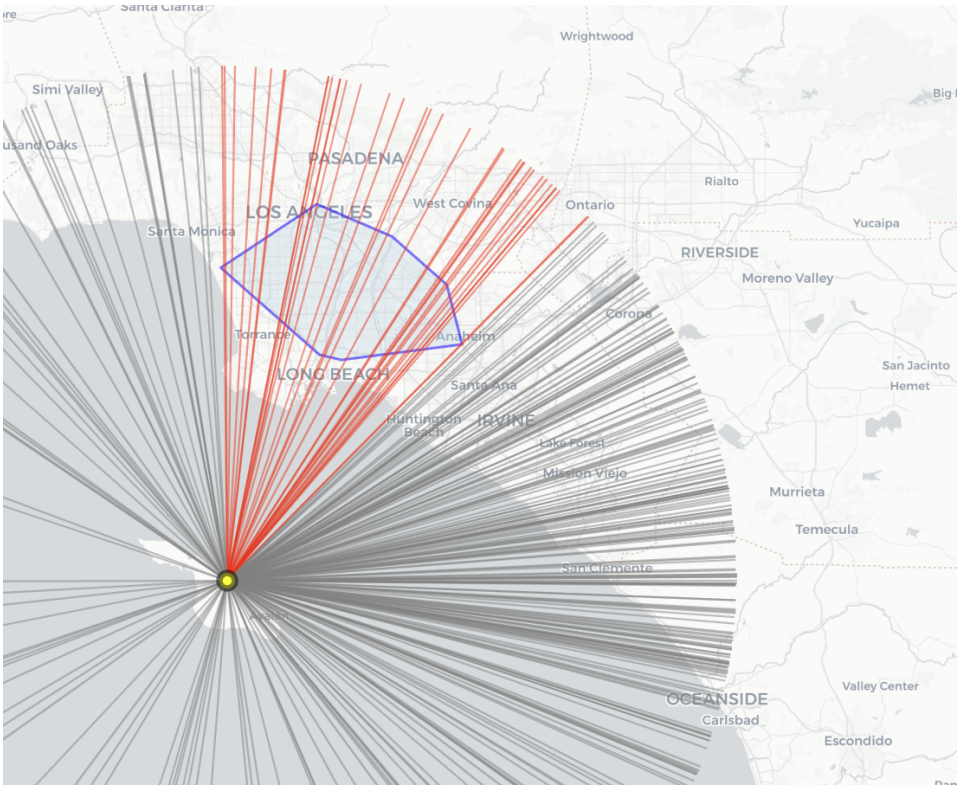
Following the zonal exposure methodology in Gillingham and Huang (2021), I define two port-proximate monitoring bands: Zone I includes monitors located within 25 miles of a port centroid, while Zone II includes those between 25 and 50 miles. Monitors beyond 50 miles are excluded from the primary analysis. These distance bins are used to compare pollutant levels across nested geographic areas that vary in proximity to port emissions sources.

To visualize exposure geography, I generate spatial plots with color-coded markers for each monitor, indicating zone assignment. Pollution measurements are aggregated to the monitor-day level, and pollutant names are harmonized across label variants. For example, entries such as "PM2.5 – Local Conditions" and "Acceptable PM2.5 AQI & Speciation Mass" are recoded under the unified label "PM2.5."

The final panel includes daily site-level concentrations for $PM_{2.5}$, PM_{10}, NO_2, NO_X, SO_2, CO, and ozone. To estimate heterogeneity in pollution exposure as a f unction of prevailing wind direction, I incorporate hourly meteorological data from the National Oceanic and Atmospheric Administration (NOAA) for 2019–2023. I extract hourly wind speed and bearing (0–360°) from six weather stations near the San Pedro Bay anchorage region, including Catalina Airport, which lies southwest of the port complex. Wind direction is defined as the origin point of air movement (e.g., 90° denotes wind from the east). Missing wind readings are imputed within station using last observation carried forward (in both forward and reverse directions).

To determine directional exposure, I compute whether each daily average wind vector intersects the convex polygon that bounds the Zone I monitors for the LA+LB port complex. For each day t, I project a geodesic line segment from the Catalina station's coordinates using the inverse of the daily wind bearing. If the projected line intersects the Zone I polygon, as displayed in Figure A6, the corresponding date is classified as a "downwind" day. This procedure yields a daily binary indicator for downwind exposure, which I merge with the monitor-day pollution panel.

Figure A6: Projected Wind Vectors and Port-Adjacent Exposure Area



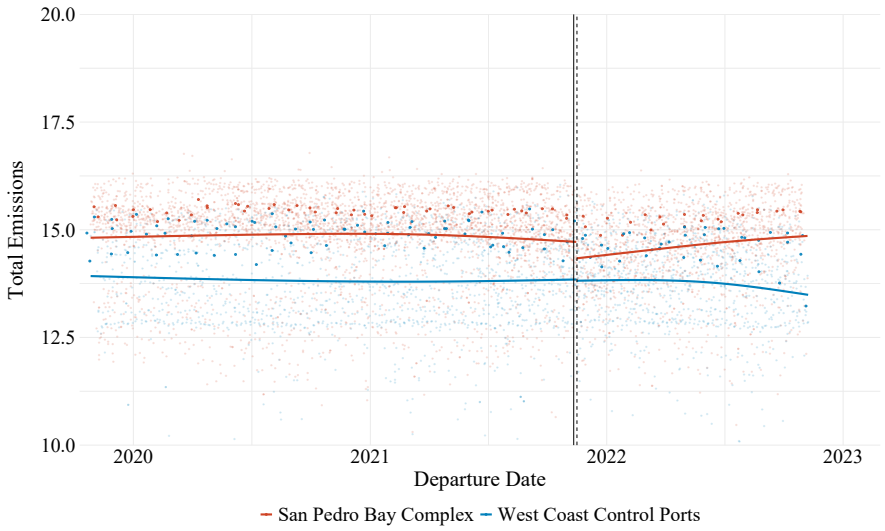
Note: Each line represents a daily-averaged wind direction originating from the Catalina Airport monitor. Red lines indicate wind vectors that intersect the defined Zone I emission polygon surrounding the San Pedro Bay port complex (Los Angeles and Long Beach). These are labeled as "downwind" days in the estimation framework. Gray lines represent non-intersecting vectors ("non-downwind" days). Base map tiles sourced from OpenStreetMap.

B Empirical Appendix

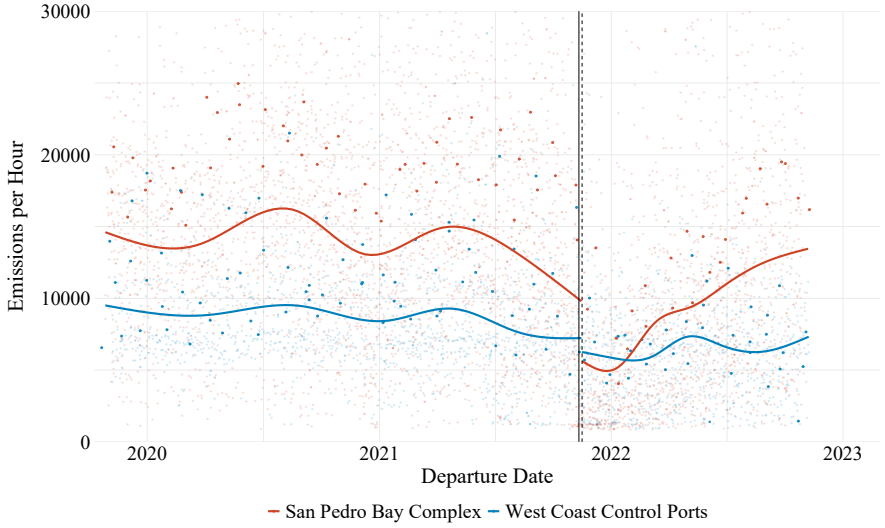
B1. Parallel Trends Assumption

Figure B7: Voyage-Leg Activity

(a) Total Emissions, Logged



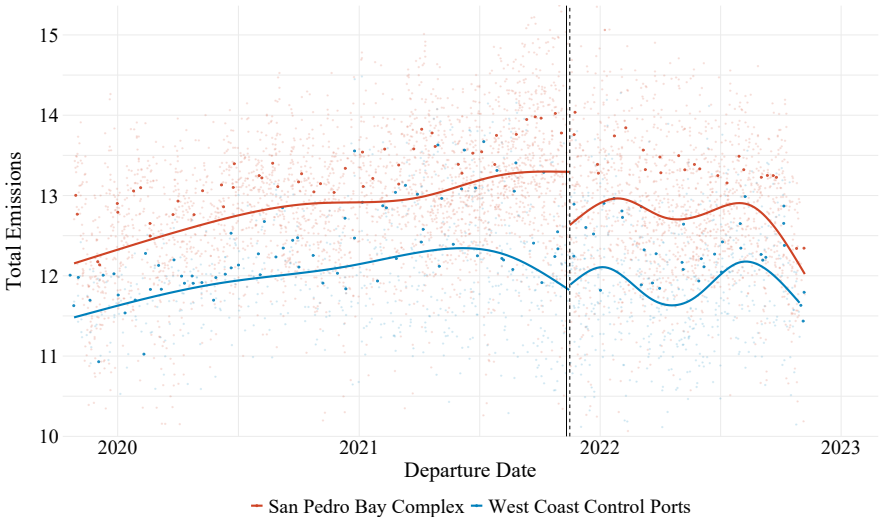
(b) Emissions per Hour



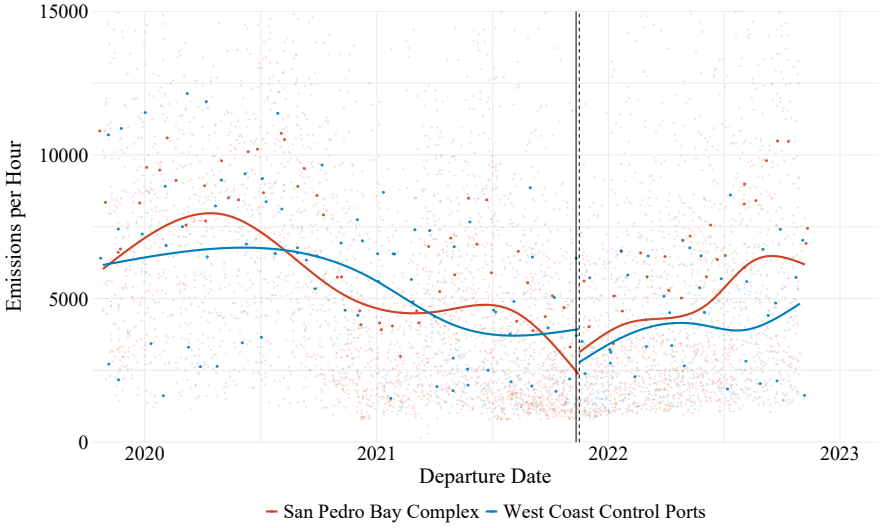
Note: Containership voyage speeds destined for San Pedro Bay (red) and control the ports of Seattle, Tacoma, and Oakland (blue). The vertical solid line marks the earliest announcement of the new queuing system (November 11, 2021). The vertical dashed line marks the start of the system's implementation (November 16, 2021). Solid lines show separately estimated restricted cubic spline functions for the periods before and after the queueing system implementation, and within San Pedro Bay and control port areas. The panel y-axis has been truncated to aid visual inspection, though the spline functions are estimated on the full sample of observations.

Figure B8: Queue-Leg Activity

(a) Total Emissions, Logged



(b) Emissions per Hour



Note: Containership voyage speeds destined for San Pedro Bay (red) and control the ports of Seattle, Tacoma, and Oakland (blue). The vertical solid line marks the earliest announcement of the new queuing system (November 11, 2021). The vertical dashed line marks the start of the system's implementation (November 16, 2021). Solid lines show separately estimated restricted cubic spline functions for the periods before and after the queueing system implementation, and within San Pedro Bay and control port areas. The panel y-axis has been truncated to aid visual inspection, though the spline functions are estimated on the full sample of observations.

B2. DiD – All International Voyages

I relax the sample to allow for vessels that are rotated across various routes. I both broaden my sample size and obtain relatively similar results to those in Tables 4 and 5.

Table B2: Difference-in-Difference Estimates – Voyage Emissions

	Total Emissions (1)	Duration (2)	Speed (3)	Em. per Knot (4)	Distance (5)	Em. per Hour (6)
Post–Period	-0.0532	-0.2067**	0.2215***	-0.0770	0.0239	0.1445
	(0.0780)	(0.0888)	(0.0783)	(0.0705)	(0.0336)	(0.1238)
Treatment	0.0822**	-0.0115	0.0423*	0.0513	0.0309**	0.0936*
	(0.0364)	(0.0252)	(0.0237)	(0.0326)	(0.0136)	(0.0552)
DiD	-0.0964**	0.1659***	-0.1620***	-0.1007***	0.0042	-0.2627***
	(0.0435)	(0.0377)	(0.0330)	(0.0389)	(0.0181)	(0.0658)
Vessel–Voyage FE	✓	✓	✓	✓	✓	✓
Year–Month FE	✓	✓	✓	✓	✓	✓
Observations	5,785	5,785	5,785	5,785	5,785	5,785
R^2	0.95	0.89	0.71	0.89	0.98	0.83

Note: ***: 0.01, **: 0.05, *: 0.1. Standard-errors are robust to clustering within vessel–voyage lanes of transport service. Each observation is a distinct international voyage experience of a vessel arriving on the US west coast between Nov 2019 and Nov 2022. To limit extreme outlier distortions, I exclude any voyages with emissions less than the 25th percentile minus three times the interquartile range (75th percentile - 25th percentile) or higher than the 75th percentile plus three times the interquartile range (Davies and Jeppesen, 2015).

Table B3: Difference-in-Difference Estimates – Queuing Emissions

	Total Emissions (1)	Duration (2)	Speed (3)	Em. per Knot (4)	Distance (5)	Em. per Hour (6)
Post–Period	-0.4646**	-0.5030**	0.0733	0.1206	-0.5852**	0.0384
	(0.1969)	(0.2179)	(0.1507)	(0.1542)	(0.2306)	(0.0920)
Treatment	0.7243***	0.8548***	-0.4183***	-0.3460***	1.070***	-0.1305**
	(0.0970)	(0.1082)	(0.0746)	(0.0776)	(0.1296)	(0.0539)
DiD	-0.2125***	-0.2865***	0.3617***	-0.3787***	0.1662*	0.0741
	(0.0754)	(0.1000)	(0.0801)	(0.0755)	(0.0946)	(0.0563)
Vessel–Voyage FE	✓	✓	✓	✓	✓	✓
Year–Month FE	✓	✓	✓	✓	✓	✓
Observations	5,090	5,090	5,089	5,090	5,090	5,090
R^2	0.70	0.70	0.72	0.66	0.63	0.78

Note: ***: 0.01, **: 0.05, *: 0.1. Standard-errors are robust to clustering within vessel–voyage lanes of transport service. Each observation is a distinct queuing experience of a vessel arriving on the US west coast between Nov 2019 and Nov 2022. To limit extreme outlier distortions, I exclude any voyages with emissions less than the 25th percentile minus three times the interquartile range (75th percentile - 25th percentile) or higher than the 75th percentile plus three times the interquartile range (Davies and Jeppesen, 2015).

Figure B9: Event Study (TWFE) - Emissions per hour

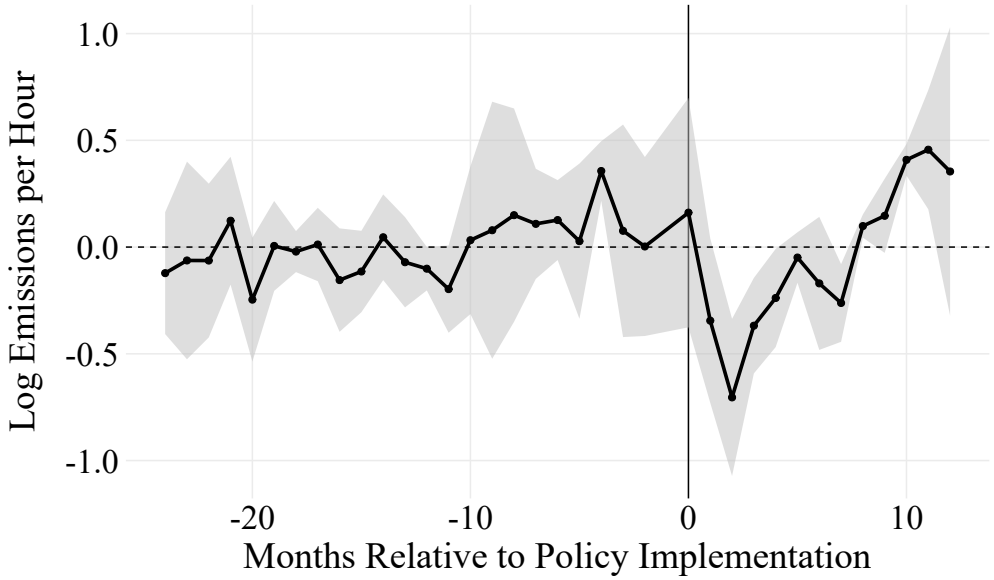


Table B4: Difference-in-Difference Estimates – Global Emissions

	CO_2 Emissions (1)	Em. per Hour (2)	Em. per Knot (3)
Post–Period	-0.1980***	0.3240***	-0.0454
	(0.0741)	(0.0929)	(0.0738)
Treatment	0.1225***	-0.0556	-0.0863***
	(0.0383)	(0.0508)	(0.0321)
DiD	-0.0980**	-0.1131*	-0.1398***
	(0.0385)	(0.0585)	(0.0412)
Vessel–Voyage FE	✓	✓	✓
Year–Month FE	✓	✓	✓
Observations	5,226	5,226	5,226
R^2	0.94	0.85	0.81

Note: ***: 0.01, **: 0.05, *: 0.1. Standard-errors are robust to clustering within vessel–voyage lanes of transport service. Each observation is a distinct global transit experience of a vessel arriving on the US west coast between Nov 2019 and Nov 2022. To limit extreme outlier distortions, I exclude any voyages with emissions less than the 25th percentile minus three times the interquartile range (75th percentile - 25th percentile) or higher than the 75th percentile plus three times the interquartile range (Davies and Jeppesen, 2015).

These findings strongly support those of the main section of the paper, which suggests that strategic route switching behaviour to avoid the new queuing system did not occur at a broad scale. This is likely due to scheduling frictions and contractual obligations limiting the ability of transport operators to remap routes within a year of this unanticipated policy introduction. Instead, the large number of switchers, entrants, and exiters appears to be business as usual. Vessels are routinely rotated across distinct shipping routes with the goal of maximizing container capacity usage (Wang et al., 2013).

B3. Air Quality Monitoring and Wind Direction

I list results of the DiD on a wider set of air quality monitor readingsa and find additional evidence supportive of port-adjacent air quality worsening relative to regions further out from the San Pedro Bay Complex.

Table B5: Difference-in-Difference, Control: San Pedro Bay, Zone-II

Dep. Variable:	CO (1)	NO2 (2)	NOx (3)	Ozone (4)
Post–Period	0.0976 (0.2539)	0.1382 (0.1670)	0.2977 (0.2551)	-0.2403 (0.1635)
Treated	0.0189 (0.0031)	-0.0392** (0.0014)	0.0819*** (0.0012)	-0.1824*** (0.0001)
DiD	0.1089** (0.0019)	0.1213*** (0.0015)	0.1121*** (0.0013)	0.0386*** (4.14×10^{-5})
Day FE Month-Year FE	✓ ✓	✓ ✓	✓ ✓	✓ ✓
Observations R^2	17,804 0.30	21,127 0.33	21,141 0.32	18,294 0.49

Note: ***: 0.01, **: 0.05, *: 0.1. Standard-errors are robust to clustering by monitor zone. Each observation is a distinct day-monitor-port emission type reading. 'Post-Period' is equal to 1 for dates November 11th 2021 to October 30th 2022. 'Treatment' is equal to 1 for air pollutant concentration monitors within a 25-mile radius (Zone I) of the centroid of the San Pedro Bay port complex. The relevant control group consists of monitors within 25-50 miles of the same reference point (Zone II).

Table B6: Difference-in-Difference, Control: Seattle/Oakland, Zone-I

Dep. Variable:	CO (1)	NO2 (2)	NOx (3)	Ozone (4)
Post–Period	0.3445** (0.0639)	0.3377** (0.0639)	0.5386** (0.1071)	-0.4985** (0.0712)
Treated	-0.2141* (0.0502)	0.3427** (0.0579)	0.3074 (0.1054)	0.2007*** (0.0078)
DiD	0.1577*** (0.0078)	0.1085** (0.0145)	0.1864*** (0.0019)	0.0402** (0.0073)
Day FE Year–Month FE	✓ ✓	✓ ✓	✓ ✓	✓ ✓
Observations R^2	17,788 0.29	21,738 0.41	20,732 0.36	17,385 0.41

Note: ***: 0.01, **: 0.05, *: 0.1. Standard-errors are robust to clustering by monitor zone. Each observation is a distinct day-monitor-port emission type reading. 'Post-Period' is equal to 1 for dates November 11th 2021 to October 30th 2022. 'Treatment' is equal to 1 for air pollutant concentration monitors within a 25-mile radius (Zone I) of the centroid of the San Pedro Bay port complex. The relevant control group consists of monitors within 25 miles of the Port of Seattle and the Port of Oakland.

In my difference-in-differences estimation, I use daily average wind direction measures stemming from an island southwest of the San Pedro Bay anchorage zone

to implement a triple difference strategy (DiDiD). I compare treated and control zones across pre- and post-policy periods, conditional on whether the region was downwind of queuing vessels on a given day.

Formally, the estimating equation is:

$$\log(Y_{izpt}) = \alpha + \gamma_1 \text{Did}_{zt} + \gamma_2 \text{Downwind}_t + \gamma_3 (\text{Did}_{zt} \times \text{Downwind}_t) + \delta_z + \lambda_{my} + \varepsilon_{izpt}$$

where Y_{izpt} is the daily average pollutant concentration at monitor i in zone z, located near port p on date t; δ_z and λ_{my} denote zone fixed effects and month-by-year fixed effects, respectively.

By focusing on variation in exposure conditional on wind direction, this approach helps distinguish local pollution impacts caused by vessel activity from broader regional trends in air quality.

Table B7: Triple Difference, Control: San Pedro Bay, Zone-II

Dep. Variable:	CO (1)	NO2 (2)	NOx (3)	Ozone (4)
DiD	0.2229 (0.0801)	0.2944 (0.0875)	0.3171 (0.1034)	0.0127* (0.0016)
Downwind	0.0809 (0.0212)	0.0760 (0.0575)	0.0847 (0.0659)	0.0190 (0.0047)
Post–Period	0.1038 (0.2489)	0.1374 (0.1556)	0.2957 (0.2418)	-0.2356 (0.1630)
Treated	0.0191 (0.0031)	-0.0391** (0.0014)	0.0820*** (0.0011)	-0.1824*** (0.0002)
DiD × Downwind	-0.1569 (0.1073)	-0.2376 (0.1181)	-0.2815 (0.1402)	0.0356** (0.0021)
Day FE	✓	✓	✓	✓
Year–Month FE	✓	✓	✓	✓
Observations	17,804	21,127	21,141	18,294
R^2	0.30670	0.33114	0.32134	0.48829

Note: ***: 0.01, **: 0.05, *: 0.1. Standard-errors are robust to clustering by monitor zone. Each observation is a specific emission type reading for a distinct day-monitor-port. 'Post-Period' is equal to 1 for dates November 11th 2021 to October 30th 2022. 'Treatment' is equal to 1 for air pollutant concentration monitors within a 25-mile radius (Zone I) of the centroid of the San Pedro Bay port complex. 'Downwind' is equal to 1 for days in which the average wind direction − calculated from hourly readings at Catalina Island − indicates that winds are blowing from outside toward the centroidal boundary of the San Pedro Bay port complex, thereby carrying emissions into the 25-mile area (Zone I) containing the monitors. The relevant control group consists of monitors within 25-50 miles of the same reference point (Zone II).

Table B8: Triple Difference: San Pedro Bay, Zone-II

Dep. Variable:	PM_{10} (1)	$PM_{10-2.5}$ (2)	$PM_{2.5}$ (3)	SO2 (4)
DiD	0.3683	0.1973*	0.1393	0.0749
	(0.0754)	(0.0239)	(0.0785)	(0.0920)
Downwind	0.1200	0.0792**	0.1820	0.0370
	(0.0519)	(0.0058)	(0.0404)	(0.0197)
Post–Period	-0.1782**	0.3084	-0.3229	0.3649**
	(0.0086)	(0.0580)	(0.2056)	(0.0240)
Treated	-0.3148***	-0.5801***	0.0033	-0.4552*
	(0.0019)	(0.0035)	(0.0014)	(0.0370)
DiD × Downwind	-0.1878	-0.0687	-0.1188	-0.2339
	(0.1073)	(0.0311)	(0.1154)	(0.0781)
Day FE	✓	✓	✓	✓
Year–Month FE	✓	✓	✓	✓
Observations	6,949	1,303	14,471	3,853
R^2	0.22125	0.40325	0.26357	0.19047

Note: ***: 0.01, **: 0.05, *: 0.1. Standard-errors are robust to clustering by monitor zone. Each observation is a distinct day-monitor-port emission type reading. 'Post-Period' is equal to 1 for dates November 11th 2021 to October 30th 2022. 'Treatment' is equal to 1 for air pollutant concentration monitors within a 25-mile radius (Zone I) of the centroid of the San Pedro Bay port complex. 'Downwind' is equal to 1 for days in which the average wind direction – calculated from hourly readings at Catalina Island – indicates that winds are blowing from outside toward the centroidal boundary of the San Pedro Bay port complex, thereby carrying emissions into the 25-mile area (Zone I) containing the monitors. The relevant control group consists of monitors within 25-50 miles of the same reference point (Zone II).

Table B9: Triple Difference, Control: Seattle/Oakland, Zone-I

Dep. Variable:	CO (1)	NO2 (2)	NOx (3)	Ozone (4)
DiD	0.2676***	0.1871***	0.3101***	-0.0492
	(0.0165)	(0.0163)	(0.0169)	(0.0176)
Downwind	0.0152	-0.0072	-0.0011	-0.0126**
	(0.0150)	(0.0092)	(0.0094)	(0.0014)
Post–Period	0.3448**	0.3341**	0.5345**	-0.4977**
	(0.0645)	(0.0655)	(0.1099)	(0.0740)
Treated	-0.2140*	0.3427**	0.3074	0.2007***
	(0.0502)	(0.0579)	(0.1054)	(0.0078)
DiD × Downwind	-0.1510**	-0.1079	-0.1699**	0.1226**
	(0.0224)	(0.0421)	(0.0223)	(0.0280)
Day FE	✓	✓	✓	✓
Year–Month FE	✓	✓	✓	✓
Observations	17,788	21,738	20,732	17,385
R^2	0.28698	0.40638	0.35839	0.41138

Note: ***: 0.01, **: 0.05, *: 0.1. Standard-errors are robust to clustering by monitor zone. Each observation is a distinct day-monitor-port emission type reading. 'Post-Period' is equal to 1 for dates November 11th 2021 to October 30th 2022. 'Treatment' is equal to 1 for air pollutant concentration monitors within a 25-mile radius (Zone I) of the centroid of the San Pedro Bay port complex. 'Downwind' is equal to 1 for days in which the average wind direction – calculated from hourly readings at Catalina Island – indicates that winds are blowing from outside toward the centroidal boundary of the San Pedro Bay port complex, thereby carrying emissions into the 25-mile area (Zone I) containing the monitors. The relevant control group consists of monitors within 25 miles of the Port of Seattle and the Port of Oakland.

Table B10: Triple Difference, Control: Seattle/Oakland, Zone-I

Dep. Variable:	PM_{10} (1)	$PM_{10-2.5}$ (2)	$PM_{2.5}$ (3)	SO2 (4)
DiD	0.3422**	0.9566***	-0.0222	-0.2105
	(0.0566)	(0.0055)	(0.0235)	(0.1301)
Downwind	0.0363	0.0761**	0.0510	0.0131
	(0.0325)	(0.0023)	(0.0575)	(0.0128)
Post–Period	0.0191	-0.3122	0.4389	0.1937
	(0.2707)	(0.2576)	(0.3753)	(0.1432)
Treated	0.5947	1.428***	0.5538**	-0.2623**
	(0.2530)	(0.0049)	(0.1095)	(0.0508)
DiD × Downwind	-0.0760	-0.0488*	0.0458	-0.1569*
	(0.0425)	(0.0042)	(0.0186)	(0.0508)
Day FE	✓	✓	✓	✓
Year–Month FE	✓	✓	✓	✓
Observations	3,330	925	27,184	8,802
R^2	0.38376	0.71023	0.22236	0.06929

Note: ***: 0.01, **: 0.05, *: 0.1. Standard-errors are robust to clustering by monitor zone. Each observation is a distinct day-monitor-port emission type reading. 'Post-Period' is equal to 1 for dates November 11th 2021 to October 30th 2022. 'Treatment' is equal to 1 for air pollutant concentration monitors within a 25-mile radius (Zone I) of the centroid of the San Pedro Bay port complex. 'Downwind' is equal to 1 for days in which the average wind direction − calculated from hourly readings at Catalina Island − indicates that winds are blowing from outside toward the centroidal boundary of the San Pedro Bay port complex, thereby carrying emissions into the 25-mile area (Zone I) containing the monitors. The relevant control group consists of monitors within 25 miles of the Port of Seattle and the Port of Oakland.